NASA Technical Memorandum 110203

Thermoplastic Ribbon-Ply Bonding Model

J. A. Hinkley
Langley Research Center, Hampton, Virginia

J. M. Marchello and B. C. Messier
Old Dominion University, Norfolk, Virginia

January 1996

National Aeronautics and
Space Administration
Langley Research Center
Hampton, Virginia 23681-0001

Thermoplastic Ribbon-Ply Bonding Model

Jeffrey A. Hinkley
Composites and Polymers Branch
NASA Langley Research Center
Hampton, VA

and
Joseph M. Marchello
and
Bernadette C. Messier
College of Engineering
Old Dominion University
Norfolk, VA

Abstract

With thermoplastic matrix resins, "on-line" consolidation of continuous-fiber composite laminates offers the potential of eliminating the post-placement autoclave or oven curing step, thereby simplifying the process and reducing costs. The aim of the present work was to identify key variables in rapid weld-bonding of thermoplastic tow (ribbon) and their relationship to matrix polymer properties and to ribbon microstructure. Theoretical models for viscosity, establishment of ply-ply contact, instantaneous (Velcro) bonding, molecular interdiffusion (healing), void growth suppression, and gap filling were reviewed and synthesized.

Consideration of the theoretical bonding mechanisms and length scales and of the experimental weld/peel data allow the prediction of such quantities as the time and pressure required to achieve good contact between a ribbon and a flat substrate, the time dependence of bond strength, pressures needed to prevent void growth from dissolved moisture and conditions for filling gaps and smoothing overlaps

Table of Contents

1.0 Introduction

Automated placement of unidirectional tape or tow is increasingly applied for the fabrication of composite structures. With thermoplastic matrix resins, "on-line" consolidation offers the potential of eliminating the post-placement autoclave or oven curing step, thereby simplifying the process and reducing costs.

A typical thermoplastic tow placement head uses hot gas or lasers to heat a shaped, pre consolidated tow just as it meets the substrate. Then a hot shoe, belt, or roller, presses the tow down as it cools, Figure 1. The consolidation cycle thus consists of a rapid heat-up to the neighborhood of the polymer degradation temperature, followed by a fairly rapid cooling as pressure is applied, Figure 2. On the next pass of the robot head, the top ply is again heated to the processing temperature. Previously-laid plies below experience a thermal wave as the process heat diffuses down into the laminate being built up, Figure 1. The sequential heating waves produce a step-wise increase in the inter-laminate bonding, Figure 3, [1,2].

The consolidation of thermoplastic plies is quite different from the processing of a typical thermoset laminate, even in a conventional press-molding or autoclave operation. The viscosity of the thermoplastic is much higher, so large-scale resin flow and squeeze-out are effectively inhibited. Instead, the consolidation or welding must be regarded as occurring in two stages: achievement of intimate contact (wetting) between the surfaces being brought together; and interdiffusion of polymer chains at the boundary -- also known as autohesion or healing at the interface.

On-line consolidation has been achieved for the filament winding of closed parts [3] and significant effort is currently being expended toward accomplishing on-line consolidation during automated tow placement, ATP, [4,5], which is applicable to a wider range of open and closed part geometry. In conjunction with the experimental effort, models describing on-line consolidation are being developed to guide the research effort and to provide a basis for machine control systems.

The consolidation models serve to relate machine design, operating parameters, and sensor readings to the processing conditions necessary for making good quality composite parts. Tow placement rate, heat flux, temperature and compactor pressure are some of the model parameters utilized in the machine control system. The purpose of the controls system is to ensure that optimal bonding conditions are provided during placement. An understanding of *in-situ* bonding, which deals with the polymer flow and molecular chain diffusion, is important in developing the process control systems needed for successful on-line consolidation [6-8].

The *in-situ* bonding kinetics model presented here draws upon past and current modeling efforts. It also utilizes the results of weld-peel experiments and the related morphological examination of the tow and weld bonds [2,9]. This information provided vital insight into the process and served as the basis for

modifying current models in developing this comprehensive model of *in-situ* tow bonding.

1.1 Dimensions

As an introduction to discussing features of ATP processing that rely on bonding models, some consideration should be given to the scale of the variables and model parameters. Perhaps the most important scale issue is the overriding concern that to be economically viable, thermoplastic ATP must operate at production rates which require the heating and compaction intervals to be at the most a few seconds in duration.

A comprehensive *in-situ* bonding model must deal with a wide range of dimensions that require shifts between discrete and continuum mechanics. For example, diffusion bonding occurs by polymer chain "reptation" at the nanometer level and utilizes molecular weight and relaxation distributions to describe the process at the micrometer and higher levels. On the other hand, the intimate contact model was originally developed at the millimeter level. It was assumed that a statistically significant number of micrometer sized fibers were present so as to justify the use of a fiber-matrix viscosity. For ATP ribbon, the scale for intimate contact is reduced to the micrometer level and the fibers must be viewed individually.

Assessment of the pressure requirements for minimization of various types of voids leads to the conclusion that for thermoplastic ribbon, tow-tow gaps and overlap ridges will require the highest compaction pressure. The ribbon dimensions are at the millimeter level and the problem lends itself conceptually to a new application of the original intimate contact model.

1.2 Placement Zone

ATP is inherently an unsteady state operation. All of the action occurs in a brief interval and over a short distance, Figure 1. In the placement zone, the temperature is increased rapidly to levels that give rise to concerns about polymer degradation, and then it is decreased to below Tg before the compaction pressure is removed.

As shown in Figure 2, both the temperature and pressure profiles vary over the length of the placement zone. At the front of the zone, heat applied to the tow and laminate begins the process of polymer softening or melting and void formation. This heating step is immediately followed by the application of pressure. Intimate contact is achieved shortly after pressure is applied and is followed by autohesion bonding which proceeds until the zone is cooled below T_g. Throughout the compaction period, pressure is exerted to contain and minimize voids.

The width of the placement zone depends upon the width of the tows and the number of tows being placed, and can change during tow cut and add operations. To ensure that all tow-tow gaps and ridges are compressed while in

the placement zone, the compactor is slightly wider than the band of tows. At any distance along the zone length, the processes occurring across the width are uniform. In passing across the tow band array width, there are sequentially the flat ribbon-ply regions and then tow-tow gaps or overlap ridges.

1.3 "On-Line" Consolidation

The *in-situ* bonding models serve to establish a processing window bounded by the upper and lower limiting values of the processing conditions within which good quality composites may be made. In principle [1], on-line sensors that monitor processing conditions during tow placement send information to the computer controller. The control program utilizes elements of the bonding model to assess where the system is in the processing window and determines what operating adjustments may need to be made.

2.0 Intimate Contact

When two surfaces are brought into contact, there is immediate adhesion arising from the effects of surface work changes, but the adhesive strength achieved by this process is relatively low [10]. For the adhesive strength to approach the polymer strength, there must be an interchange of material across the interface by some sort of diffusion process. For this process to occur, there has to be intimate contact between the surfaces.

2.1 Ply Surface Roughness

Current on-line consolidation modeling draws on the intimate contact model proposed by Dara and Loos [11] as refined by Lee and Springer [12]. Composite laminates are formed by laying up unidirectional plies of prepreg. Since the ply surfaces are uneven, gaps are present between plies prior to the application of heat and pressure. Thermoplastic matrix resins do not flow into the gaps because of their high melt viscosities, so to attain intimate contact between adjacent surfaces, the surface roughness must be deformed.

For modeling purposes, it is assumed that the ply roughness may be represented as rectangular ridges comprised of unidirectional fibers and polymer, Figure 4. The degree of intimate contact, D_{ic}, is

$$D_{ic} = b/(w_0+b_0) \qquad (1)$$

b_0 and b are the initial and instantaneous widths of roughness elements, and w_0 is the initial distance between adjacent elements. Since the element volume is constant, for unit length, $v_0 = a_0 b_0 = a\, b$

$$D_{ic} = (a_0 / a)/(1+w_0 b_0) \qquad (2)$$

For conservation of mass in the control volume of width dy, Figure 4,

$$a\, du_y/dy + da/dt = 0 \qquad (3)$$

y is the coordinate along the interface and t is time. For laminar flow of the resin-fiber system into the gap between roughness elements [12]

$$u_y = -(a^2 / (12\, \mu_{mf})\, (dP / dx) \qquad (4)$$

where μ_{mf} is the viscosity of the fiber-polymer mixture. If the scale of the deformation is greater than the distance of a fiber from the surface [13]

$$\mu_{mf} = \frac{\mu}{\left[1-\sqrt{\left(V_f / \mathcal{F}\right)}\right]} \qquad (5)$$

V_f is the fiber volume and $\mathcal{F}$ is the packing factor.

Combining Equations 3 and 4 and integrating with the conditions $P = P_e$ at $y=b/2$ gives

$$P - P_e = (6\, \mu_{mf} / a^3)(da/dt)\, [y^2 - b/2)^2] \qquad (6)$$

For a ply of length A and width B under a force F, the force applied per unit length of roughness element is

$$f = (F/A)(1/n)$$

and the number of elements

$$n = B / (b_0 + w_0)$$

giving

$$f = (F/(A\, B))(b_0 + w_0) = P_{app}\, (b_0 + w_0) \qquad (7)$$

where P_{app} is the applied pressure. The force applied to an element is balanced by the pressure inside

$$f = \int_{-b/2}^{b/2} (P - P_e)\, dy \qquad (8)$$

Combining Equations 6, 7, and 8 and integrating using constant or average values for t and P gives [12]

$$\frac{a_0}{a} = [1 + \frac{5P_{app}}{\mu_{mf}}(1 + \frac{w_0}{b_0})(\frac{a_0}{b_0})^2 t]^{1/5} \qquad (9)$$

Dropping the assumption of constant T and P, and using Equation 2 gives the relationship developed by Mantell and Springer [8] for the degree of intimate contact

$$D_{ic} = \frac{1}{(1+\frac{w_0}{b_0})}[1+5(1+\frac{w_0}{b_0})(\frac{a_0}{b_0})^2\int_0^{t_{ic}}\frac{P_{app}}{\mu_{mf}}dt]^{1/5} \qquad (10)$$

The tow placement process is nonisothermal. In fact, it involves very rapid and significant changes in temperature and pressure, as was shown in Figure 2. Linear viscoelasticity theory offers a basis for evaluating the time integral of P_{app}/μ_{mf}. The total response during a nonisothermal process with any temperature profile $T = \Theta(t)$ is equivalent, via the Boltzmann Superposition Principle, to a hypothetical isothermal experiment of duration

$$t_{eff} = \int_0^{t_{ic}} du / [a(\Theta(u), T_0)] \qquad (11)$$

where t_{eff} is an effective time and $a(T,T_0)$ is the time-temperature shift factor relative to the reference temperature T_0.

If T_0 is chosen to be T_g, the "Universal" WLF expression

$$log[a(T,T_g)] = -17.44(T-T_g)/(51.6 + T - T_g) \qquad (12)$$

may apply, and the integration in Equation 10 can then be performed for a given temperature profile [2].

Assuming that the integral in Equation 10 is evaluated in keeping with viscoelastic theory, and that P and μ_{mf} values are calculated as weighted averages over the placement interval, then the time for intimate contact, which occurs when $D_{ic} = 1$, can be obtained by rearranging Equation 10 to give

$$t_{ic} = (\frac{\mu_{mf}}{5P_{app}})(\frac{1}{(1+\frac{w_0}{b_0})})(\frac{b_0}{a_0})^2[(1+\frac{w_0}{b_0})^5 - 1] \qquad (13)$$

In their experimental verification of Equations 10 and 13, Lee and Springer [12] measured, as a function of molding time, temperatures and pressures,.the degree of intimate contact with metal mold plates that was achieved by plies of APC-2 From their degree of intimate contact data, reproduced in Figure 5a, they obtained agreement with Equation 10 by using $w_0/b_0 = 1$, $a_0/b_0 = 0.3$ and

$$\mu_{mf} = 1.14x10^{-12}[exp(26300/T] \text{ Pa-s} \qquad (14)$$

The corresponding time to reach intimate contact, Figure 5b, varied with pressure and temperature. At 382°C and 50 psi, for example, the time for intimate contact is about 30 seconds.

The expression used by Lee and Springer [12] for the neat resin (PEEK 150P) viscosity in their impregnation model, was

$$\mu = 1.13x10^{-10}[exp(19100/T)] \text{ Pa-s} \qquad (15)$$

The important role of viscosity in intimate contact may be illustrated from Equations 14 and 15. At 382 °C, the matrix-fiber viscosity from Equation 14 is μ_{mf} = 31,260 Pa-sec, and the neat resin viscosity from Equation 15 is μ = 520 Pa–sec, so that $\mu_{mf}/\mu = 60$. Since intimate contact is proportional to viscosity (Equation 9), the contact time would be reduced from 30 sec. to as little as 0.5 seconds if the surfaces were polymer rich.

The difficulty in assessing Equation 5 for the matrix-fiber viscosity, is illustrated by Mantell and Springer's use of the expression [8]

$$\mu_{mf} = 132.95[exp(2969 / T] \text{ Pa-s} \qquad (16)$$

for APC-2 in place of Equation 14. They retained the use of Equation 15 for the PEEK. At 382 °C, Equation 16 gives μ_{mf} = 602 Pa-s. That is, Equations 14 and 16 differ by over 50-fold in their predictions of μ_{mf}.

2.2 ATP Ribbon Roughness

To date, the modeling of intimate contact has assumed the roughness element to be comprised of many fibers impregnated with polymer. That is an appropriate model for the surface of prepreg tape, but it is not for ATP ribbon. The thermoplastic ribbons used in ATP are consolidated tows with roughness elements having dimensions on the order of one fiber as may be seen from Figures 6 and 7.

For a roughness element comprised of one fiber coated with polymer, flow leading to intimate contact occurs in molten polymer, so μ should be used in Equations 10 and 13. If it is assumed that to a first approximation, $w_0 = b_0 = a_0$, then the time for intimate contact becomes

$$t_{ic} = (\mu/(5P_{ic}))(1/2)(1)[(2)^5 - 1] \qquad (17)$$

$$= 3.1(\mu/P_{ic})$$

where P_{ic} is the pressure required to achieve intimate contact. Equation 17 is proposed as the model for intimate contact of thermoplastic tows during automated placement.

In the discussion of Equation 13 above, it was observed that if the neat resin viscosity were used, the intimate contact time for PEEK plies, at 381 °C and 50 psi, would be reduced from 30 seconds to 0.5 seconds. As an example of the use of Equation 17, consider a polymer having a viscosity of 10,000 Pa-s. If the time to achieve intimate contact is to be 0.1 seconds, the pressure that must be applied may be calculated to be

$$P_{ic} = =(3.1)(10{,}000)/(0.1) = 310\ kPa = 45\ psi$$

An intimate contact time of 0.1 seconds and an applied pressure of 45 psi are attractive values in making sandwich structure (which requires skin placement on honeycomb core).

2.3 Polymer Crystallinity

While matrix crystallinity in the final composite is included in most models [14], the role of polymer crystallinity in achieving intimate contact during ATP is not. Some insight into the development of bond strength is provided by studies of the heat sealing of polyethylene films [15]. Experiments indicate that film seal initiation begins abruptly for polyethylenes at the temperature for which the polymer is 77% amorphous. That is, to obtain good seal bonds, the films must have less than 23% crystallinity, and bond quality falls off sharply at higher levels of crystallinity. This finding is consistent with the Dahlquist criterion for pressure-sensitive adhesives [16].

In the model of film sealing [15], the surface of a film is rough on a microscopic scale, and the films are initially in intimate Van der Waals contact at only a fraction of the apparent contact area. When heat is applied, melting of the crystalline polymer occurs, and the application of slight pressure causes increased molecular contact, or wetting, of the molten film surfaces. Given sufficient time, polymer-chain segments from opposite sides of the interface diffuse across the interface and create molecular entanglements between molecules in the interfacial zone. Subsequently, cooling and crystallization occur, yielding a heat sealed joint.

Most of the polymers used in ATP have a fairly low degree of crystallinity. For example, PIXA tows have heats of melting on the order of 5 J/g, while the PIXA perfect crystal has a heat of melting of 139 J/g [17]. Thus, the PIXA matrix is less than 5% crystalline. Also, the melting temperature range for polyimides is smaller than that of polyethylenes. In view of this, it is not proposed to include a polymer crystallinity component in the ATP intimate contact model. However, the heating and cooling illustrated in Figure 2 may be too rapid for melting to occur. In this case, crystalline polymer surface areas would fail to wet and bond, resulting in a reduction in composite properties.

2.4 Fiber Deformation

The process for making thermoplastic ATP tow ribbons involves consolidation and shaping while the impregnated tow is under significant tension [1,18].

Therefore, fiber non-alignment and waviness might not be expected to be an important factor in achieving intimate contact. However, scanning electron micrographs of the ribbon surfaces, Figure 8, show some degree of fiber non-alignment. During unidirectional placement, surface fiber non-alignment could result in the need for higher consolidation pressure and would serve to create voids in the composite. In addition, when plies are being placed in other than unidirectional orientations, fiber deformation at the gaps between adjacent tows of the previously placed ply is a concern in achieving intimate contact and void free composites.

Fiber curvature and non-alignment, and the resulting fiber deformation during ATP, are not included in current ATP models [4,6,19], but they are part of a filament winding model [20]. The fiber deformation model proposed by Gutowski [21] was used by Carpenter and Colton [20] to formulate a model for thermoplastic filament winding. Two mechanisms, polymer flow parallel to the fibers and fiber bed compaction, are assumed to occur during the formation of intimate contact and the removal of entrapped air as the tow passes through the compaction region.

In assessing the value of incorporating elements of a filament winding model into the ATP intimate contact model, it is important to bear in mind the differences between filament winding and ATP. In winding, the tow is not cut and the parts have convex surfaces. ATP endeavors to be applicable to any part geometry, including concave sections. Also, with ATP there is tow cut and add which greatly reduces the tow tension that can be applied during placement. Both methods use essentially the same heating sources and pressure application devices.

The Carpenter and Colton model determines the applied force, F, using the relationship

$$F = W\int_0^L [P_m(x) + P_f(x)]dx \qquad (18)$$

where W is the tow width, x is the position along the compaction length, $P_m(x)$ is the polymer matrix pressure drop for flow, $P_f(x)$ is fiber bed pressure. The applied pressure $P_{app} = F/WL$. $P_m(x)$ is obtained from D'Arcy's law with the Kozeny-Carmen permeability expression and the Carreau model for shear-thinning fluids. The expressions for these factors may be represented by a μ_{mf} term like that employed in Equation 6.

The primary difference between these models is in the coordinate systems. Lee and Springer [12] use a fixed coordinate system and integrate over the time for heating and compaction at a given position in space, Equation 10. Carpenter and Colton use a moving coordinate system and integrate over the length of the heating and compaction zone, Equation 18. The end result is the same in that x and t are related to the linear placement rate, $U = x/t$.

The fiber bed pressure distribution [20] is described by

$$P_f(x) = \frac{c\sqrt{\frac{V_f(x)}{V_0}} - 1}{\left(\sqrt{\frac{V_\infty}{V_f(x)}} - 1\right)^4} \qquad (19)$$

where c is a spring constant for the fiber bed; c = 159 Pa for APC-2 [19]. V_∞ is the highest fiber volume fraction attainable, V_0 refers to the initial fiber volume fraction, and $V_f(x)$ is the fiber volume fraction at position x along the compaction zone.

The value to ATP modeling of the Carpenter and Colton model for filament winding lies in establishing the way to include tow surface fiber non-alignment and tow-tow gaps during placement of angle plies. As part of an on-line consolidation model, Equations 18 and 19 in Equation 10 provide a general expression for the degree of intimate contact. The time to achieve intimate contact, Equations 13 and 17, also would utilize properly averaged values of μ and P_{app}.

2.5 Summary: ATP Intimate Contact

The model for ATP intimate contact discussed above is depicted in Figure 6. Heating melts the surface polymer, which flows under the compaction pressure to fill surface roughness gaps. In addition, fibers move laterally due to the applied pressure to fill gaps. Non-aligned fibers may inhibit this movement and angle plies may not fill tow-tow gaps in the underlying layer. Either of these factors may give rise to voids. The model for intimate contact during tow placement is expressed by the relationship

$$t_{ic} = 3.1\ (\mu / P_{ic}) \qquad (17)$$

with the applied pressure being the sum of the polymer flow pressure and the fiber deformation pressure averaged over the time to achieve intimate contact. Similarly, the polymer viscosity is the average over the time-temperature interval, Equation 11. Examination of this expression for representative values of μ and P_{ic} suggests that for automated placement of thermoplastic ribbon, the time to achieve intimate contact is of the order of 0.1 seconds.

3.0 Interfacial Bonding

When two samples of the same or compatible polymers are brought into contact at a temperature above their glass transition temperature, the junction gradually develops increasing strength until the full fracture strength is reached. At this

point, if the polymers are identical, the interface is no longer distinguishable and the samples are fully bonded.

3.1 Autohesion

The diffusional process that takes place across the polymer-polymer interface derives from the random molecular motion at temperatures greater than T_g. The molecular motion in entangled polymer melts is described by three components [10]. They are a longitudinal displacement by reptation, segmental transverse reorganization of the chain, and rotational movement in the chain. These form an overall chain motion that may be characterized by a three-dimensional diffusion coefficient.

The diffusion of molecular chain segments across an interface gives rise to an inter-penetration of chains and to the formation of physical links between molecules from different sides of the interface. This process of polymer interfacial healing or welding is described by the polymer molecular chain reptation theory of de Gennes and Edwards [16].

In the reptation model of molecular chain movement, entanglement with adjacent chains imposes a constraint upon the chain which restricts lateral motion. That is, the chain is confined to move backward and forward along a curvilinear length, or tube, and only the chain ends can exit the tube. Because the chain ends are free to move in a random direction away from the tube, the initial tube position in space is gradually lost. The ends of the chain that have relaxed from their original position are referred to as minor chains [22]. The reptation time is the interval over which the chain completely loses its original configuration.

Since de Gennes proposed it in 1971, the reptation model has been experimentally confirmed and the theory refined and extended by a number of investigators. These include adjustments for minor chain models, nonlinear chains, interface crossing frequency analysis, and a nonisothermal shift factor [4,6,22,23,24].

Reptation theory predicts that the degree of autohesion is proportional to the one-fourth power of the time lapse from when intimate contact was established, and proportional to the molecular weight to powers ranging from 1/2 to 5/4 depending on the range of molecular weights [16]. In their theoretical assessment of the time dependence of the crossing density, and in related experiments, Prager and Tirrell [23] found that the dependency is to the one-half power of time if the initial contact is between surfaces which have been equilibrated against a gas phase. Alternatively, if the contacting surfaces contain many chain ends, such as might be found at fracture surfaces, the time dependency is to the one-fourth power.

With the exception of Loos and Li [6], who use a one-half power time dependency in their non-isothermal autohesion model, most modelers express the time growth of interfacial bond strength using a reptation-based one-fourth power time relationship of the form

$$\frac{H(t)}{H(\infty)} = \left(\frac{t}{t_r}\right)^{1/4} \qquad (20)$$

where $H(t)$ is the interfacial bond strength at time t, $H(\infty)$ is the ultimate bond strength or fracture strength of the polymer, and t_r is the reptation time.

The reptation time is related to temperature by the Arrhenius equation. In the chain relaxation distribution, reptation represents the longest relaxation time, which corresponds to the time, t_r, needed for a chain to escape from its original tube. In terms of molecular quantities, Doi [25] gives

$$tt_r = \frac{\zeta \beta^2 N^3}{\pi^2 k_B T N_e} \qquad (21)$$

where N is the number of segments in the chain, β is the segment length, T is absolute temperature, k_B is Boltzmann's constant, N_e is the number of segments between entanglements, and ζ is a friction constant related to diffusion in the melt.

In his study, Agarwal [26] reviewed the difficulties with earlier attempts to measure the reptation time of polymer melts. From rapid compression molding experiments, he determined the time required for consolidation of APC-2 to be rapid, less than 7 seconds. In mapping his non-isothermal processing data to isothermal conditions, Equation 11, the bonding time at 400 °C for APC-2 was estimated to be approximately 0.1 seconds. From rheometric experiments, the relaxation time for PEEK 150G was determined to be 0.04 seconds at 390 °C, which compares well with a bonding time of 0.1 seconds at 400 °C. From reptation theory, Agarwal calculated that the relaxation times range from 10^{-4} seconds for the low molecular weight chains in the melt to 100 seconds for the higher molecular weight chains.

3.2 Molecular Velcro

The immediate adhesive strength arising from the effects of surface work changes when two surfaces are brought into contact is low, unless there is some initial molecular interchange across the interface [10]. Upon contact of two polymer surfaces, there is the possibility of an initial exchange of molecular chains at the surface.

Most of the autohesion, or healing, experimental studies have dealt with contact times ranging from 1 to 100 minutes, and the scatter of the data has been such as to justify simple extrapolation to zero bonding at zero time [6,10,12]. An exception is the studies of Hinkley and co-workers [2,9] who used IR heating to study composite ribbon welding at heating times as short as five seconds. Their data imply the possibility of initial contact bonding with strengths as high as one-quarter that obtained for complete welding.

In their molecular Velcro model of the initial bonding process, O'Conner and McLeish [27] considered the dynamics of the process in three stages: rapid network penetration; mode relaxation; and co-ordinate hopping. In network penetration the chain becomes embedded in the surface layer chain network. Once in this layer, the chain may tunnel immediately or diffuse in the layer. During mode relaxation the chain may back-track down its current tube, or tunnel into a new tube. During co-ordinate hopping the chain end moves from the end of its initial tube to the end of a new tube. These three stages for the surface contact dynamics lead to a "mushroom" conformation in which a polymer chain is partially in both surfaces and there is a "mushroom" of coiled chain in the interfacial network layer.

In explaining molecular Velcro, McLeish [28] points to the difference in energy dissipated in fastening and unfastening a Velcro strip: there is a great deal of noise as the tangled fibrous strips are pulled free, and silence as they are pushed together. At the molecular level, the driving force is not applied pressure, but entropy in that the chain has more configuration in the bulk than on the surface. Once chains have made an initial penetration across the interface, they get stuck in a metastable state leaving a "plume" or "mushroom" of polymer that must reptate, or diffuse, further to complete the bonding process. This model may help account for observed short-time bonding.

3.3 Ultimate Bond Strength

Although autohesion is controlled by a diffusional process, the achievement of full bonding occurs in a finite time rather than asymptotically. Experimental data for crack healing and autohesion bonding confirm that bonding is complete in a finite length of time [4,8,10-12,29]. Once the polymer-polymer interface has completely bonded, it has the same fracture and mechanical strength as the bulk polymer. The magnitude of the bonding time is dominated by the higher molecular weight fraction of the polymer [24].

3.4 Summary: ATP Interfacial Bonding

At a given interfacial location, the build up of bond strength begins once intimate contact has been established between the two surfaces and proceeds through the reptation time interval. Based on the autohesion and molecular Velcro models, a semi-empirical expression for the time dependence of the bond strength would be

$$\frac{H(t)}{H(\infty)} = \left(\frac{H(0)}{H(\infty)}\right) + \left(\frac{t - t_{ic}}{t_r}\right)^{\nu} \qquad (22)$$

where: $H(0)/H(\infty)$ is the degree of instantaneous Velcro bonding, t is the total time under pressure, $(t\text{-}t_{ic})$ is the reptation time interval, and ν is either 1/4 or 1/2.

From the available information, it is likely that $0 \leq H(0)/H(\infty) \leq 0.25$ and that $0.1 \leq t_r \leq 100$ seconds. These quantities may be determined empirically for the temperatures and polymer molecular weight distribution to be used in the ATP process by fitting to Equation 22.

Because of the sensitivity of t_r to molecular weight and molecular weight distribution, control of batch-to batch variations may be a critical issue in achieving reliable and reproducible composite processing by in-situ ATP consolidation.

4.0 Composite Voids

The quality of a composite is inversely proportional to its void content. Thermoplastic ATP utilizes fully consolidated tows that are nearly void free. During the tow placement process, however, voids may appear both within the tows and at the tow-tow surfaces. Intra-ribbon voids can result from internal changes in the tow ribbon due to entrapped or dissolved air, water and other volatiles, and possibly from the release of fiber stresses upon softening of the matrix. Volume changes accompanying polymer melting are another possible source. Inter-ribbon voids may occur at the tow-tow gaps (due to the failure of tow deformation to fill gaps during placement) and may also occur between plies (as a result of failure to achieve full intimate contact between the surfaces of the tow being placed and the previously-placed ply).

4.1 Intra-ribbon Voids

Heating to melt the polymer on the tow surface begins prior to the application of compaction pressure, Figure 2. During this brief interval the polymer softens and thermally expands and any crystallinity that it has probably melts. In the process, the polymer loses strength and releases carbon fiber stresses, dissolved volatiles and entrapped air. This results in void formation in the tow. The subsequent application of compaction pressure serves not only to stop void creation, but to reverse it.

Void formation and equilibrium stability models [1,20,30-32], utilizing phase nucleation and diffusion controlled growth theory, predict the pressure required, at a given temperature, to contain and eliminate voids in composites. For void growth to occur, the void pressure must be larger than the polymer hydrostatic pressure plus the surface tension forces.

$$P_g \geq P_e + \left(\frac{\gamma_{LV}}{m_{LV}}\right) \qquad (23)$$

where: P_g is the void pressure, P_e is the polymer pressure, γ_{LV} is the surface tension between the polymer and the void, and m_{LV} is the ratio of void volume and surface area of the void.

Voids in composites have been extensively studied and modeled [30,31]. Primary concern focuses on the role of air and water in the voids. Kardos [30] proposed the relationship between void pressure and temperature

$$P_g = P_a + x_1 P_1 \qquad (24)$$

where: P_a is the partial air pressure, which increases linearly with temperature; x_1 is the water concentration in the resin; and P_1 is the water vapor pressure, which increases exponentially with temperature.

The compaction pressure, transmitted via P_e, needed to overcome P_g and thereby to contain void formation may be determined from Equations 23 and 24. For example, at 350 °F and 2% moisture, P_g = 60 psia [31]. At these processing conditions, surface tension has been found to play a relatively minor role [20].

Fiber bed pressure, Equation 19, may be used to analyze voids arising from fiber deformation stresses that may be in the consolidated ribbon and released during heating. Because the ribbon is made from unidirectional fibers under tension, voids from this source are felt to be of minor concern. This assumption is borne out from micrographs of welded ribbon, Figure 9, which show bubble type voids. It is possible that they were nucleated at fiber stress points.

4.2 Inter-ribbon Voids

Due to the variations in tow width, there are gaps between adjacent tows that must be filled, either by lateral deformation of the tow during initial placement, or by vertical deformation during subsequent placement passes [1]. Many ATP operations program the controller to provide a small degree of ribbon overlap to avoid gaps. The resulting overlap ridge must be flattened to eliminate voids and provide a smooth laminate surface. There is also the potential for interlaminar voids, or delaminations, due to failure to achieve full intimate contact between plies.

The processing conditions needed for intimate contact and to reduce edge voids and ridges may be determined from Equation 17. Tow deformation is depicted in Figure 4 and described by Equation 13. As an illustration of the use of Equation 13 to predict the required compaction pressure, consider tow-gap dimensions of w_0 = 0.010 inches, b_0 = 0.250 inches, and a_0 = 0.005 inches. Substituting into Equation 13 gives

$$t_{ic} = 77.8(\mu_{mf} / P_{ic}) \qquad (25)$$

If μ_{mf} = 10,000 Pa-s and the gap is to be filled in 0.5 seconds, then P_{ic} = 220 psia. This is the pressure that must be exceeded by the compactor to eliminate the tow-tow gaps. Depending on the extent of overlap, a somewhat lower pressure would be needed to flatten a ridge.

A comparison of Equations 17 and 25 indicates that void minimization requires higher pressure than wetting. Using t_{ic} in Equation 25 is conservative in that the gap filling is assumed to be achieved during wetting. The gap closure period could be extended into the reptation interval. This would reduce the required pressure, but would risk lower composite properties due to incomplete bonding.

4.3 Summary: APT Void Model

The ATP compaction device plays a key role in minimizing void content in the composite. It must provide pressure in excess of the pressures of the voids that may arise in the tow as it is heated and it must force ribbon deformation flow into the tow-tow gaps.

Equations 24 and 13 suggest that for the nearly moisture-free tow ribbon used in ATP, tow internal voids require less compression pressure than is required for tow deformation into gaps or to smooth overlap ridges at the ribbon edges. Consequently, the ATP void model utilizes Equation 13 in the form

$$P_{gv} = \left(\frac{\mu_{mf}}{5t_{ic}}\right)\left(\frac{1}{\left(1+\frac{w_0}{b_0}\right)}\right)\left(\frac{b_0}{a_0}\right)^2\left[\left(1+\frac{w_0}{b_0}\right)^5 - 1\right] \qquad (26)$$

where: P_{gv} is the pressure needed to minimize voids in the composite, b_0 is the tow width, a_0 is the tow thickness and w_0 is the tow-tow gap or the ridge width. μ_{mf} is a function of ribbon dimensions and polymer viscosity, Equation 5.

5.0 Comprehensive Ribbon-Ply Bonding Model

For thermoplastic ATP, the proposed tow-ply bonding model is comprised of three elements: intimate contact, interfacial bonding, and void minimization. The phenomenological features of these processes were discussed earlier and are quantified by the expressions:

Intimate contact

$$t_{ic} = 3.1(\mu/P_{ic}) \qquad (17)$$

Interfacial bonding

$$\frac{H(t)}{H(\infty)} = \left(\frac{H(0)}{H(\infty)}\right) + \left(\frac{t - t_{ic}}{t_r}\right)^v \qquad (22)$$

Void minimization

$$P_{gv} = (\frac{\mu_{mf}}{5t_{ic}})(\frac{1}{(1+\frac{w_0}{b_0})})(\frac{b_0}{a_0})^2[(1+\frac{w_0}{b_0})^5 - 1] \qquad (26)$$

These equations describe the role of polymer, fiber, and tow properties in the placement process. The viscosity and reptation time relate temperature and molecular weight to the wetting, or intimate contact, time and to bonding and processing pressure.

To complete the ATP modeling process for making a specific composite product, these model relationships must be incorporated into solutions to the differential heat transfer equations, with appropriate machine- and product-specific boundary conditions. The following observations from Equations 17, 22, and 26 indicate the general model features and how they relate to ATP composite manufacturing.

In the design and operation of ATP machines, business considerations such as production cost minimization are expected to dictate placement rate, tow dimensions and tow band width. Polymer properties establish the temperature levels (T_g, T_m, and the degradation temperature) within which the polymer viscosity and reptation time are determined, with proper allowance for the non-isothermal nature of the operation, Equation 12.

From consideration of the machine and product dimensions, a practical upper limit may be placed on the length of the placement zone. Using the established placement rate, the total available time interval may then be determined as the zone length times the placement speed. This placement time is the sum of an initial pre-compression heating interval, the time for establishment of intimate contact, the reptation time, and a cooling interval at the end of the compression, Figure 2. The time above T_g is comprised of t_{ic} plus t_r.

The choice of heat sources dictates the length of the pre-consolidation heating zone, which when subtracted from the total zone length establishes the length of the pressure compactor. The time under compaction is its length divided by the linear placement rate. The choice of compactor cooling methods sets the zone length needed to lower the temperature below Tg. The difference between the total time under compaction and the end cooling interval is the time period available for t_{ic} plus t_r. Thus, with $H(t)/H(\infty)=1$ for full bonding, all the terms in Equations 17 and 22, except P_{ic} have been established and these equations may be used to calculate the compaction pressure needed for intimate contact.

The remaining general design concern is void minimization. The pressure above which voids are minimized is given by Equation 26 , where μ_{mf} is obtained from Equation 5 and the Arrhenius relationship for the polymer viscosity, e.g. Equations 14 and 16. In the development of Equation 17 and 26, it was apparent that $P_{gv} > P_{ic}$. Thus, the choice of compactor pressure load is probably dictated by void minimization considerations, Equation 26.

In their non-isothermal autohesion model for amorphous thermoplastic composite, Loos and Li [6] incorporated a transient heat transfer analysis into a model for isothermal autohesive bond development. The two dimensional transient Fourier conduction Equation was used

$$\rho C_p \frac{\partial T}{\partial t} = \frac{\partial}{\partial x}(k\frac{\partial T}{\partial x}) + \frac{\partial}{\partial y}(k\frac{\partial T}{\partial y}) \qquad (27)$$

where ρ is the density, C_p is the specific heat, k is the thermal conductivity, T is temperature, and t is time. The isothermal autohesion model, Equation 20, with 1/2 power time dependence, was used with the WLF expression, Equation 12, to establish a non-isothermal autohesion model. A finite element program was utilized to numerically solve Equation 27 with initial and heat flux boundary conditions. The calculated temperatures were then used with Equations 12 and 20 to determine the autohesion bonding. The numerical calculations agreed well with experimental data [29].

The effects of processing conditions on void growth during thermoplastic fiber placement has been modeled by Pitchumani, Rangabathan, Don and Gillespie [32]. They identify five dominant physical mechanisms involved in the process: heat transfer, polymer degradation, intimate contact, healing and void consolidation. Numerical methods were used to solve the set of differential equations that describe the consolidation squeeze flow, the instantaneous tow thickness as it passes under the roller, and the spherical void compression. In this way, the void fraction and tow thickness were determined as a function of axial location along the process. The model was compared with experimental placement data. It was found that both the void fraction and the tow thickness increased with increasing temperature and decreasing line speed.

A similar consolidation and void reduction model developed by Ranganthan, Advani and Lamontia [19] predicts the change in void content due to applied consolidation pressure and due to the change in temperature as the tow passes under the compaction roller. Iterative numerical methods were used to develop computer solutions for the model. It was found that the required compaction pressure increased linearly with increasing tow speed, which is consistent with Equation 26.

In their discussion, Ranganthan, Advani and Lamontia [19] point out that prior to entering the compaction roller region, the tow undergoes some thermal deformation. They observe that this un-modeled process could play an important role. Ranganthan *et al.* close with the comment that one of the primary purposes for developing the model was to aid on-line control of the placement process. The computer execution time of the model was therefore critical. However, even in its most simplified form, the model takes too long for its predictions to be of use on-line. The model has been run off-line for various parameters in the processing window and a computer look-up table constructed that can then be used as to guide on-line control.

6.0 Ribbon Weld-Peel Experiments

In conjunction with the development of the *in-situ* bonding kinetics model, rapid tow welding experiments were conducted. These tests were primarily directed toward confirmation of Equation 22. Cross sectional micrographs of the welds also shed light on the void growth process.

An experimental setup capable of bonding ribbons in a few seconds [2,9] was used. The ribbons contained IM7 fiber and either a thermoplastic polyimide or a phenylethynyl-terminated imide oligomer.

6.1 Materials

IM7 fiber (Hercules) impregnated with PIXA polymer (Mitsui) was obtained from Cytec. PETI-5 powder-coated tow was prepared at NASA LaRC. Both materials were ribbonized at LaRC. The consolidated ribbons were about 6 mm (0.25 inches) in width and were supplied on a continuous spool. Specimens were cut at approximately 15 cm (6 inch) lengths.

Several specimens were weighed separately and then dried at 200°C for 14 hours. After drying, the ribbons were weighed again to determine if any residual solvents and moisture had evaporated. The PIXA ribbon showed less than 0.1% weight change. The PETI-5 ribbon averaged a weight loss of 0.41% with a range of 0.39% to 0.45%.

Glass transition temperatures of PETI-5 and PIXA are 227°C and 250°C respectively. Results from a differential scanning calorimeter (DSC) indicate the heat of melting of the polymer in the ribbon was -10.62 J/g of polymer for PETI-5 and -4.656 J/g of polymer for PIXA.

6.2 Equipment and procedures

Figure 10 is a schematic view of the welding apparatus. An infrared lamp is used to weld the ribbon while time-temperature data are obtained using three 0.55 mm-diameter thermocouple probes positioned along the centerline of the weld. The lamp on-time and the shutter opening and closing time are governed by a personal computer via solid-state relays. A dead weight load on the stage applies pressure to the ribbon-to-ribbon/glass sandwich. The total weld surface area and effective pressure were $4.84 \times 10^{-4} m^2$ ($0.75\ in^2$) and $21.1\ kN/m^2$ (3.06 psi) respectively.

A portion of the ribbons were drilled with three holes 0.8 mm in diameter and 1.9 cm apart. When this procedure is used, the thermocouple probes penetrate the top ribbon and rest on the bottom ribbon at the interface being welded. Because of the concern over the effect the holes might have on the peel data, another 8 pairs of ribbon were welded without pre-drilled holes for the thermocouples. In this case, the thermocouples rest on the upper surface of the upper ribbon.

Ribbon-to-ribbon welds were made with varying weld times (12,16, 20 and 24 seconds).

Three welded ribbon pairs were made for each weld time for each material. One of these welds was potted in epoxy resin, cross-sectioned, and polished for micrography using a variable speed grinder-polisher. The other two welds were peeled apart at room temperature at a rate of 1.3 cm/min to determine the weld bond strengths. The ASTM Floating Roller Peel Test, D3167-93, was used. Figure 11 depicts the test fixture and illustrates the specimen preparation for peeling. Cyanoacrylate was used to adhere one ribbon to the rigid aluminum substrate. The flexible tape on the other adherend helps to restart the peel in the event of a break in the ribbon. The tape adhesive is stronger than the ribbon-to-ribbon weld, so peeling occurs at the ribbon-ribbon weld interface.

During peeling, loads were recorded approximately 15 times/second. Figure 12 shows a typical set of peel data. Because of the scatter, a consistent procedure was adopted to determine an average peel strength: the highest one hundred data points of every thousand points were averaged. Areas of initial and final slack, unexplainable spikes and fractures were eliminated.

The ribbon surfaces and the weld peeled surfaces were sputter coated with gold-palladium alloy and examined with a Hitachi scanning electron microscope (SEM) at a magnification of 500 times.

6.3 Results and Discussion

The experimental data were analyzed to obtain information about the weld bonding process. The objective of the analysis was to determine the bonding kinetics and to evaluate the bond quality.

Scanning Electron Microscope

An initial step in bonding is to achieve wetting, or intimate contact, between the adherends. Therefore, the ribbon smoothness and surface composition is important to welding. Figures 13 and 14 show SEM photographs of PETI-5 and PIXA as received. Individual fibers are visibly coated with polymer. The PIXA ribbon surface shows that the fibers are linear with little evidence of crossover. The PETI-5 ribbon surface shows some fiber crossover.

Figures 15 and 16 are SEM photographs of the separated ribbon-glass interface of PETI-5 and PIXA at the 24 second lamp times, respectively. The glass had been painted with Frekote mold release prior to welding to facilitate removal from the glass. The figures show substantial resin flow, but incomplete contact. The shape of the menisci suggests that bubbles were trapped against the glass.

Figures 17 and 18 show SEM photographs of fracture surfaces after the peel test. PETI-5's fracture surface is characteristic of a resin which is not fully cured. The PIXA polymer is more ductile and the fracture appears to be primarily at the fiber-resin interface.

Peel Data

The time and temperature conditions for the welds are presented in Tables 1 and 2. For each polymer, thermocouples were located at the welded interface for 8 ribbon pairs as described in the Experimental section.

Table 1

Welding conditions for PETI-5 (T_g = 227 °C)

Lamp On Time seconds	Time to Reach T_{max} from T_g, seconds	Total Time Above T_g, seconds	T_{max}, °C	Effective Time t_{eff} (with respect to T_g), seconds
12	5.6	7.9	320	1.247×10^{11}
12	6.2	9.2	328	3.138×10^{11}
16	10.4	17.4	371	1.334×10^{13}
16	10.2	15.5	348	2.682×10^{12}
20	14.1	23.6	390	4.766×10^{13}
20	14.4	24.7	397	6.885×10^{13}
24	18.5	31.2	405	1.228×10^{14}
24	17.5	31.2	405	1.228×10^{14}
*12	4.2	6.3	311	3.767×10^{10}
*12	5.2	10.3	345	1.43×10^{12}
*16	7	12.2	358	4.182×10^{12}
*16	9.5	15.7	367	9.386×10^{12}
*20	13.4	21.5	384	3.24×10^{13}
*20	13.9	25.3	397	7.052×10^{13}
*24	17.4	35	418	2.304×10^{14}
*24	18.2	38.2	434	4.425×10^{14}

* Indicates those ribbons without the predrilled holes.

Table 2

Welding conditions for PIXA (T_g = 250 °C)

Lamp On Time, seconds	Time to Reach T_{max} from T_g, seconds	Total Time Above T_g, seconds	T_{max}, °C	Effective Time t_{eff} (with respect to T_g), seconds
12	3.7	4.8	310	1.037×10^{9}
12	4.6	6.1	322	8.095×10^{9}
16	8.8	11.7	357	6.77×10^{11}
16	10.2	14.6	394	1.1×10^{13}
20	12.2	19.7	404	2.549×10^{13}
20	13.3	18.9	383	7.364×10^{12}
24	17.1	27.1	415	6.013×10^{13}
24	16.8	24	409	3.995×10^{13}
*12	4.1	5.9	334	3.528×10^{10}
*12	4.5	6.4	340	7.408×10^{10}
*16	8	11	354	4.911×10^{11}
*16	8.7	11.6	367	1.494×10^{12}
*20	12.6	18.5	392	1.243×10^{13}
*20	11.6	15.4	375	3.534×10^{12}
*24	16.6	19	423	6.045×10^{13}
*24	14.7	22.9	405	3.119×10^{13}

* Indicates those ribbons without the predrilled holes.

The lamp-on times ranged from 12 seconds to 24 seconds. Welds below 12 seconds show little if any bond strength, while the bonds for 24 second heating are strong enough to fracture the ribbons during the peel test. In the course of the peel tests for those ribbons with thermocouple holes, the PIXA ribbon peeled uniformly, while PETI-5 tended to fracture . However, for the ribbons without thermocouple holes, PETI-5 peeled uniformly and the PIXA ribbon fractured.

As expected, the highest peel strengths, approximately 1.5 kN/m, were obtained for the 20 and 24 second-welded specimens. Weld strength did not correlate well with lamp heating time alone (Figure 19), primarily because the maximum temperature reached is somewhat variable. Plotting the peel data versus effective time [2,9] provided a better correlation (Figures 20 through 27). For both PIXA and PETI-5 the bond strength thresholds begin at about 0.5 kN/m; strengths increase with increasing effective time.

The peel strength data were fitted with an equation that accounted for molecular bonding rates. The general expression (Chapter 3) was:

$$P = P_0 + a(t_{eff})^n$$

where P_0 is immediate or "Velcro" bonding, and the second term is the diffusional or "reptation" bonding. The constant a should be the reciprocal of the reptation time to the $1/n$ power. The exponent n is either 1/4 or 1/2 depending upon the condition of the surface.

The values of P_0 and a obtained by least squares fitting of the peel data (Figures 20-23) are presented in Table 3. Using χ^2 as an index of "goodness of fit", the fit is seen to be marginally better with n = 1/4.

Table 3

Fitting parameters for $P=P_0+a(t_{eff})^n$

PETI-5			
n	**a**	**P_0**	**χ^2**
1/4	1.030×10^{-4}	0.36	1.23
1/2	1.666×10^{-8}	0.48	1.41
PIXA			
n	**a**	**P_0**	**χ^2**
1/4	3.630×10^{-5}	0.69	2.22
1/2	1.605×10^{-8}	0.69	2.22

To assess the merits of the "Velcro" intercept, the data were also fit to a simple reptation model of the form:

$$P = a(t_{eff})^n$$

The results are shown in Table 4 and Figures 24 through 27.

Table 4

Fitting parameters for $P = a(t_{eff})^n$

PETI-5		
n	***a***	χ^2
1/4	2.318×10^{-4}	2.19
1/2	8653×10^{-8}	4.84
PIXA		
n	***a***	χ^2
1/4	3.731×10^{-4}	5.56
1/2	1.408×10^{-7}	7.84

Weld Cross-Sectional Micrographs

The upper-left photos in Figures 28 and 29 are of the ribbon as received; they illustrate the differences between two powder prepregging processes. The PIXA had been powder coated at Cytec and the PETI-5 at NASA LaRC. Note that the PIXA is resin rich at the surface. Both ribbons were made at NASA LaRC. In both materials, the surface roughness is of the order of magnitude a fiber diameter.

Void generation during the weld bonding process is a major concern. Figures 28 and 29 show void growth for various weld times. The infrared radiation was incident from the right side of the photographs. Note that the ribbon on the right shows more void formation. PIXA had less than 0.1% moisture and showed some bubbles. PETI-5 had 0.4% moisture and more void growth. In addition, the lower melt viscosity of PETI-5 may contribute to the difference in the size and prevalence of voids. Examination of the photographs shows that void growth appears immediately as temperatures approach Tg. Since even the lightly welded ribbons show significant voids, void generation appears to occur more rapidly than weld bonding.

6.4 Conclusions

To better understand interfacial composite bonding, thermoplastic composite ribbons were welded together using an infrared heater and then peeled apart. These tests were accompanied by optical and SEM micrographic examination of the materials and their fracture surfaces.

Bond strength was observed initially at 0.5 kN/m for both PETI-5 and PIXA ribbons. The highest measureable peel strengths, approximately 1.5 kN/m, were obtained for specimens with effective times at T_g of 10^{14}-10^{15} seconds.

SEM of fracture surfaces was helpful in examining the degree of contact.

A significant number of bubbles (voids) were observed at all degrees of welding. Weld bond strength was determined as a function of effective time at T_g. The peel strength-time data were fitted to an expression based on diffusional interfacial bonding. The data correlate slightly better with $n = 1/4$ than $n = 1/2$. The identification of an immediate bond strength supports the molecular Velcro model for initial contact. The coefficient a is related to the reptation time at T_g.

7.0 Bibliography

1. D. A. Sandusky, J. M. Marchello, R. B. Baucom and N. J. Johnston, "Customized ATP Towpreg", 24th International SAMPE Technical Conference, p T591-T605, October 1992.

2. J. A. Hinkley, D. C. Working and J.M. Marchello, "Graphite/Thermoplastic Consolidation Kinetics", 39th International SAMPE Symposium, p 2604-2611, April 1994.

3. P. Wagner and J. Colton, "On-Line Consolidation of Thermoplastic Towpreg Composites in Filament Winding", 39th International SAMPE Symposium, p 1536-1545, April 1994.

4. R. Pitchumani, R. C. Don, J. W. Gillespie, Jr., and S. Ranganathan, "Analysis of On-Line Consolidation During a Thermoplastic Tow-Placement Process", in "Heat and Mass Transfer in Composites Processing" M. K.Alam and R. Pitchumani eds., ASME Press, 1994.

5. S. K. Mazumdar and S. V. Hoa, "Determination of Optimum Processing Conditions By Taguchi Method For On-Line Consolidation of PEEK/Carbon Thermoplastic Composites", 39th International SAMPE Symposium, p 1546-1553, April, 1994,

6. A. C. Loos and M. C. Li, "Non-Isothermal Autohesion Model for Amorphous Thermoplastic Composites", Journal of Thermoplastic Composite Materials, Vol. 7, p 280-310, October, 1994.

7. M. N. Ghasemi Nejhad, "Issues Related to Processability During the Manufacture of Thermoplastic Composites Using On-Line Consolidation Techniques", Journal of Thermoplastic Composite Materials, Vol. 6, p 130-146, April, 1993.

8. S. C. Mantell and G. S. Springer, "Manufacturing Process Models for Thermoplastic Composites", Journal of Composite Materials, Vol 26, No. 16, p 2348-2376, 1992.

9. J. A. Hinkley, R. W. Grenoble and J. M. Marchello, "Rapid Welding of Thermoplastic Towpreg Ribbon", 40th International SAMPE Symposium, p 1560-1571, May 1995.

10. K. Jud, H. H. Kausch and J. G. Williams, "Fracture Mechanics Studies of Crack Healing and Welding of Polymers", Journal of Materials Science, Vol. 16, p 204-210, 1981.

11. P. H. Dara and A. C. Loos, "Thermoplastic Matrix Composite Processing Model", NASA CR-176639, 1986.

12. W. I. Lee and G. S. Springer, "A Model of the Manufacturing Process of Thermoplastic Matrix Composites", Journal of Composite Materials, Vol. 21, p 1017-1055, November, 1987.

13. R. B. Pipes, J. W. S. Hearle, A. J. Beaussart, A. M. Sastry, and R. K. Okine, "A Constitutive Relation for the Viscous Flow of an Oriented Fiber Assembly", Journal of Composite Materials, Vol. 25, p 11204-1225, 1991.

14. S. Mantell, Q. Wang and G. S. Springer, "Thermoplastic Tape Laying", 36th International SAMPE Symposium, p 1763-1772, April, 1991.

15. F. C. Stehling and P. Meka, "Heat Sealing of Semicrystalline polymer Film. II. Effect of Melting Distribution on Heat-Sealing Behavior of Polyolefins", Journal of Applied Polymer Science, Vol. 51, p 105-119, 1994.

16. L. H. Sperling, Introduction to Physical Polymer Science, p 181, 536, John Wiley & Sons, New York, 1992.

17. J. B. Friler and P. Cebe, "Development of Crystallinity in NEW-TPI Polyimide", Polymer Engineering and Science, Vol 33, No. 10, p 587-597, 1993.

18. D. A. Sandusky, J. M. Marchello, R. M. Baucom, and N. J. Johnston, "Ribbonizing Powder-Impregnated Towpreg", 39th International SAMPE Symposium, p 2612-2626, April, 1994.

19. S. Ranganathan, S. G. Advani, and A. Lamontia, "A Model for Consolidation and Void Reduction during Thermoplastic Tow Placement", 25th International SAMPE Technical Conference, p 620-631, October, 1993.

20. C. E. Carpenter and J. S. Colton, "On-Line Consolidation Mechanisms in Thermoplastic Filament Winding (Tape Laying), 38th International SAMPE Symposium, p 205-217, May, 1993.

21. T. G. Gutowski and Z. Cai, "Thermoplastic Composite Consolidation Model", ASME Manufacturing International, Vol. 4, p 13-29, 1988.

22. R. P. Wool and K. M. O'Conner, "A Theory of Crack Healing in Polymers", Journal of Applied Physics, Vol. 52, No. 10, p 5953-5963, 1981.

23. S. Prager and M. Tirrell, "The Healing Process at Polymer-Polymer Interfaces", Journal of Chemical Physics, Vol. 75, No. 10, p 5194-5918, 1981.

24. D. Adolph, M. Tirrell, and S Prager, "Molecular Weight Dependence of Healing and Brittle Fracture in Amorphous Polymers above the Entanglement Molecular Weight", Journal of Polymer Science - Physics Edition 23, 413-427 (1985)

25. M. Doi, "Molecular Rheology of Concentrated Polymer Systems I" Journal of Polymer Science - Physics Edition 18, 1005-1020 (1980)

26. V. Agarwal, "The Role of Molecular Mobility in Consolidation and Bonding of Thermoplastic Composite Materials", Ph.D. degree thesis, Center for Composite Materials, University of Delaware, 1991.

27. K. P. O'Conner and T. C. B. McLeish, " 'Molecular Velcro' - Dynamics of a Constrained Chain into an Elastomer Network", 9th International Conference on Deformation, Yield and Fracture of Polymers, p 17/1-17/4, Churchill College, Cambridge, UK, April 1994.

28. T. McLeish, "Molecular Velcro Disentangled", Physics World, Vol. 7, No. 8, p 24-25, August, 1994.

29. J. C. Howes, A. C. Loos and J. A. Hinkley, "the Effect of Processing on Autohesive Strength Development in Thermoplastic Resins and Composites", Advances in Thermoplastic Matrix Composite Materials, G.M. Newaz, ed. ASTM STP 1044, p 33-49, 1989.

30. J. L. Kardos, R. Dave and M. P. Dudukovic,, "Voids in Composites", ASME, Manufacturing International '88 Proceedings, Vol. IV, The Manufacturing Science of Composites, edited by T.G. Gutowski, 1988.

31. L. A. Berglund and J. M. Kenny, "Processing Science for High Performance Thermoset Composites", SAMPE Journal, Vol. 27, No. 2, p 27-37, 1991.

32. R. Pitchumani, S. Ranganathan, R. C. Don and J. W. Gillespie, Jr., "Effects of Processing Conditions on Void Growth During Thermoplastic Fiber Placement", Mechanics of Materials Processing and Manufacturing, T. J. Moon and M. G. Nejhads, eds., ASME Press, 1994.

Figure Captions

1. Schematic of in-situ thermoplastic tape laying or tow placement

2. Illustrative thermal and pressure cycle during laydown

3. Proposed development of interlaminar strength at a given ply boundary during repeated passes of the placement head.

4. Assumed geometry of ply/ply contact

5. Test of intimate contact squeeze flow model (data of Lee and Springer [12] on APC-2)
    a. degree of intimate contact vs. time
    b. time for complete contact at various temperatures and pressures

6. Sketch showing scale of surface roughness in preconsolidated ribbon

7. Cross section photomicrograph of PETI-5 ribbon, note smooth surfaces and lack of voids. As an indication of scale, thickness of the ply is approximately 125 μm.
8. SEM micrograph of ribbon surface.

9. Cross section of welded PIXA ribbon showing voids. Scale same as Figure 7.

10. Exploded view of welding setup.

11. ASTM roller peel fixture and preparation of ribbons for peel test.

12. Example of raw peel data. Points between the vertical lines were averaged by the procedure described in the text.

13. SEM of PETI-5 ribbon as received

14. SEM of PIXA ribbon as received

15. SEM of weld surface heated in contact with glass plate

16. SEM of weld surface heated in contact with glass plate

17. SEM of peeled surface after fracture

18. SEM of peeled surface after fracture

19. Weld peel strength vs. heating time

20. PETI-5 peel strength vs. effective time referred to Tg; fit with intercept and $n = 1/4$

21. PETI-5 peel strength vs. effective time referred to Tg; fit with intercept and n = 1/2

22. PIXA peel strength vs. effective time referred to Tg; fit with intercept and n = 1/4

23. PIXA peel strength vs. effective time referred to Tg; fit with intercept and n = 1/2

24. PETI-5 peel strength vs. effective time referred to Tg; fit with n = 1/4

25. PETI-5 peel strength vs. effective time referred to Tg; fit with n = 1/2

26. PIXA peel strength vs. effective time referred to Tg; fit with n = 1/4

27. PIXA peel strength vs. effective time referred to Tg; fit with n = 1/2

28. Cross sections of PETI-5 ribbon and welds processed at various times

29. Cross sections of PIXA ribbon and welds processed at various times

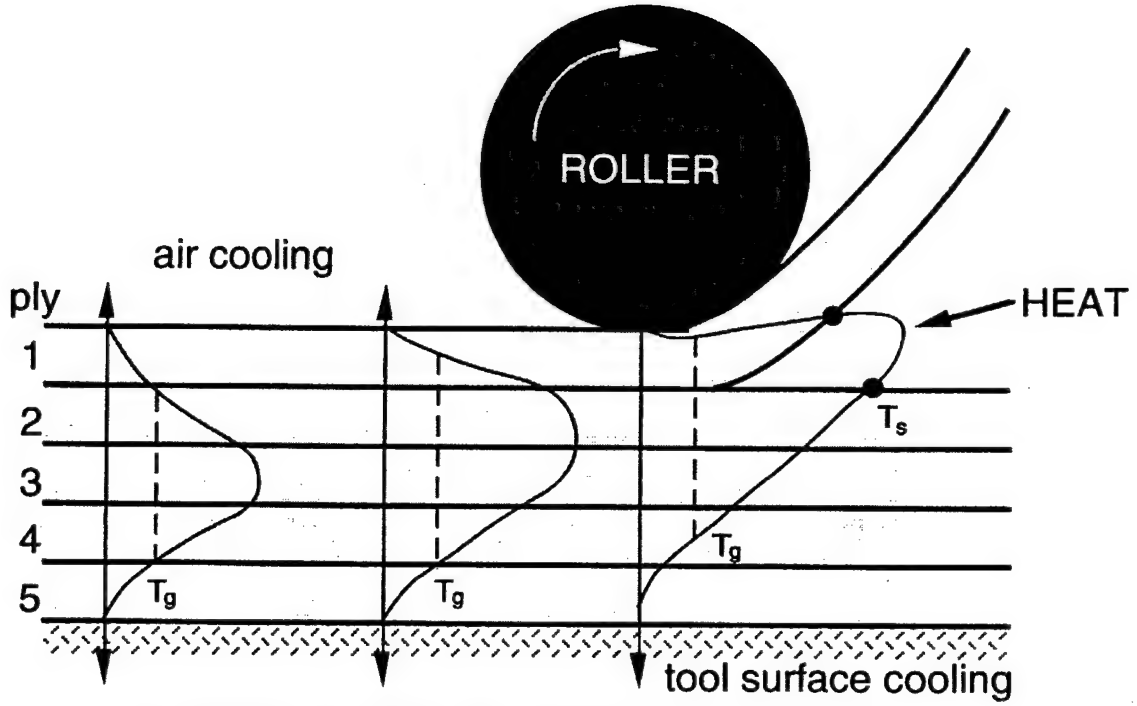

TEMPERATURE PROFILES DURING ATP

- Bonding at Ply 1 - Ply 2 interface is primarily by wetting
- Bonding at deeper ply interfaces is by diffusion when $T > T_g$

ATP HEAT WAVE BONDING MODEL

Figure 1

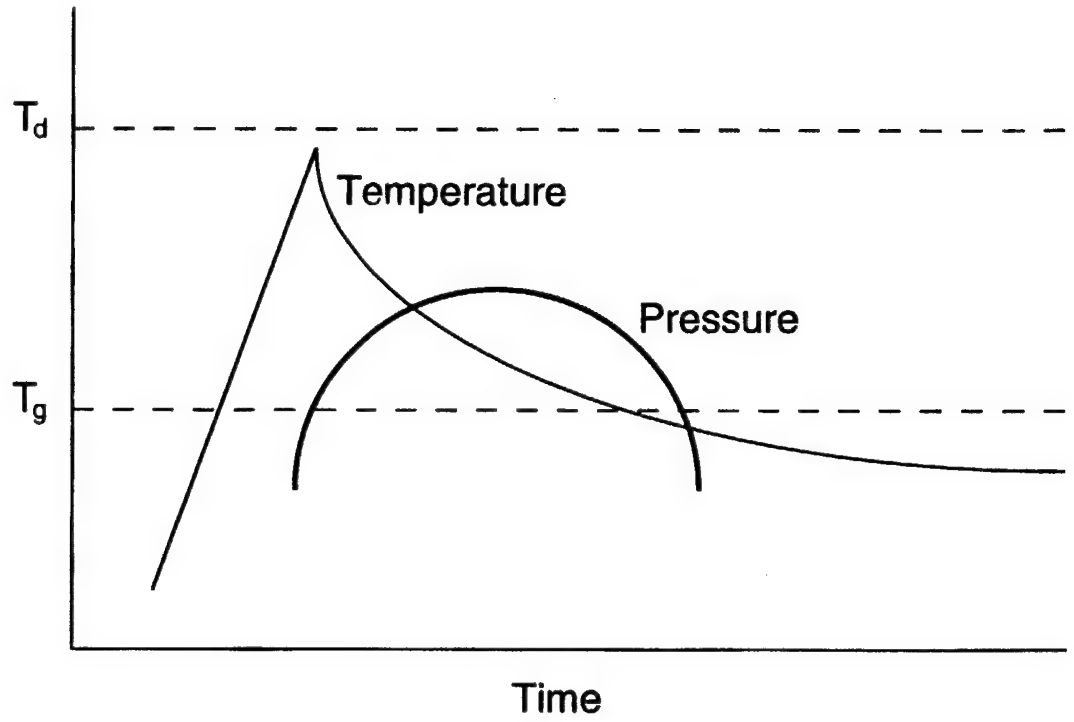

- Temperature ramp exceeds 100°C/second.
- Pressure applicator may have heated front to extend period above T_g , but it must have cooled rear to lower temperature below T_g before pressure is removed.

ATP IN-SITU CONSOLIDATION CYCLE

Figure 2

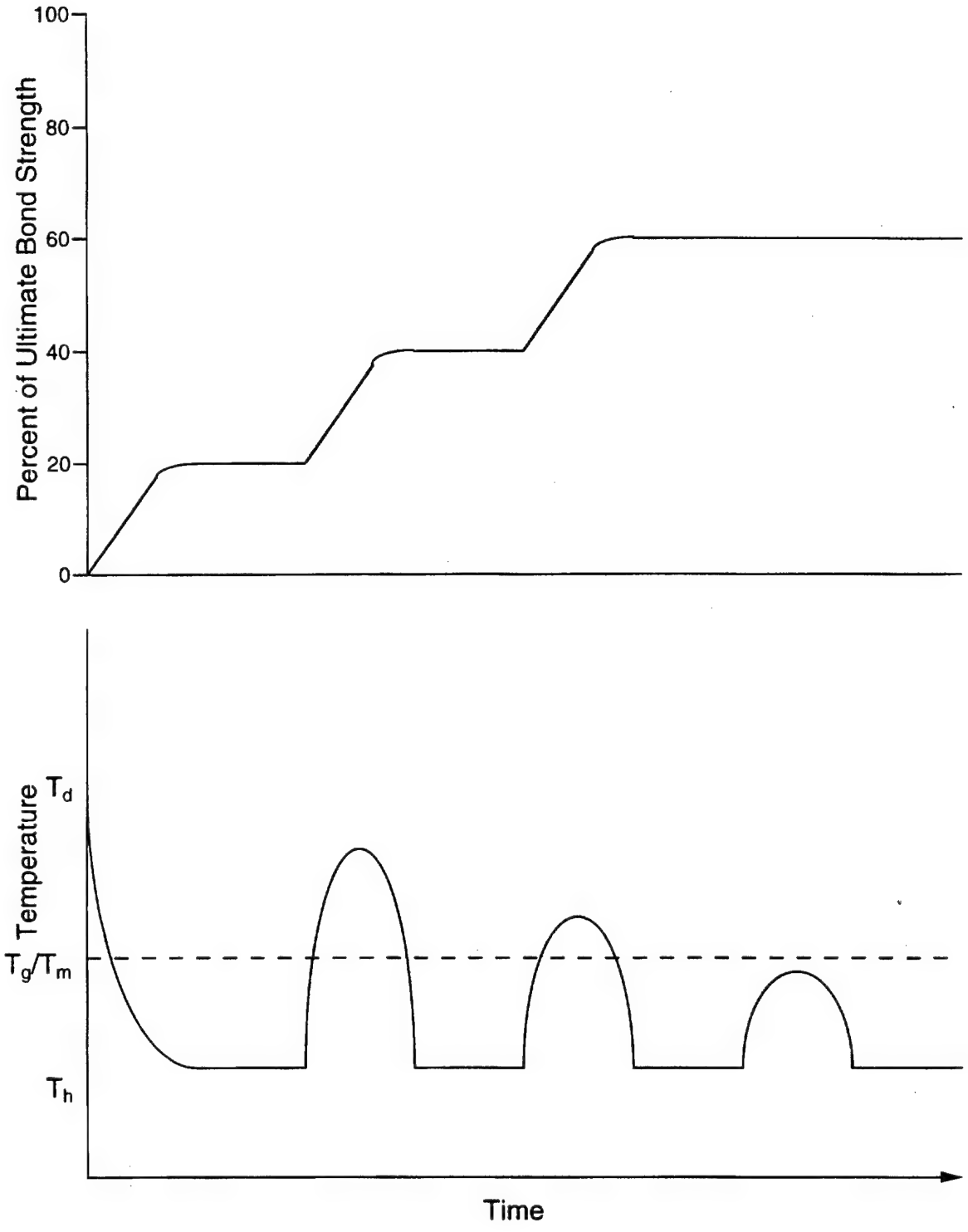

THERMAL WAVE BONDING

Figure 3

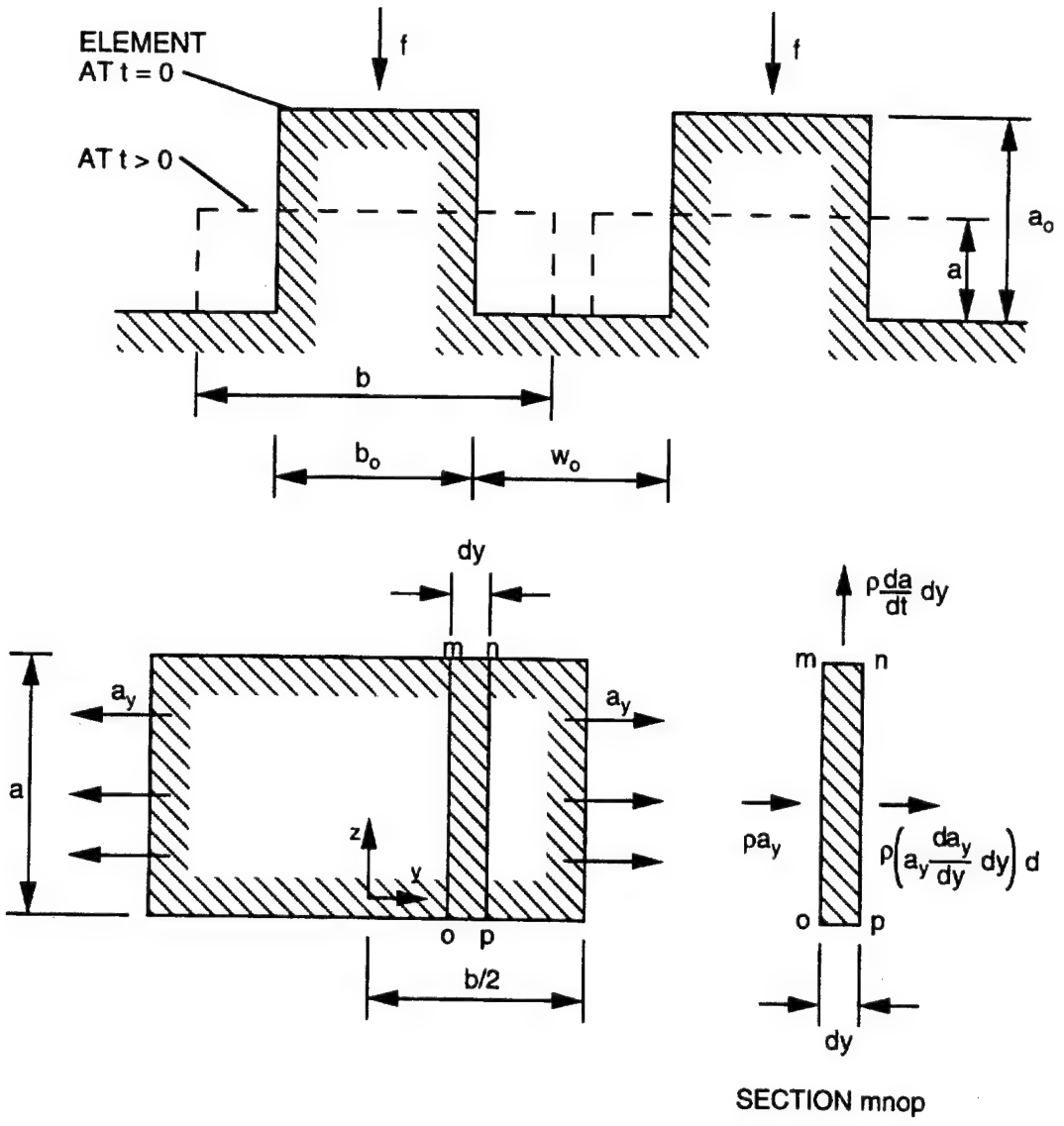

Top: Rectangular elements representing the uneven surface at time t = 0.
Bottom: Illustration of one element at time t, and the control volume used in calculating mass flows.

Figure 4

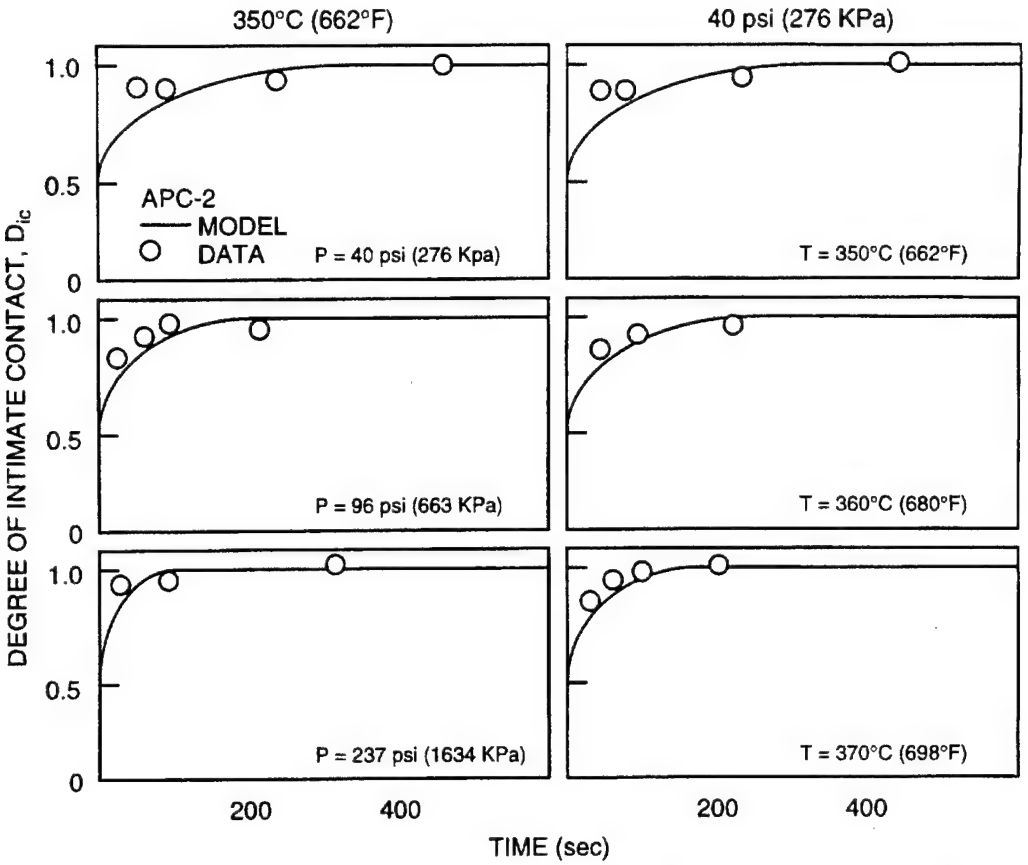

Figure 5a. Degree of intimate contact versus contact time as a function of applied temperature and pressure. Comparison of the results of the model with data.

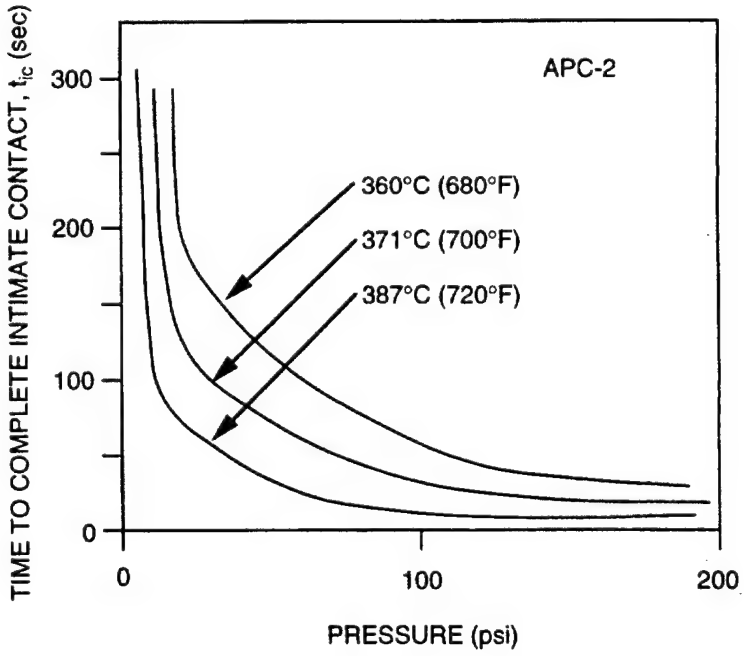

Figure 5b. Time required for complete intimate contact (D_{ic} = 1.0) versus applied temperature, pressure.

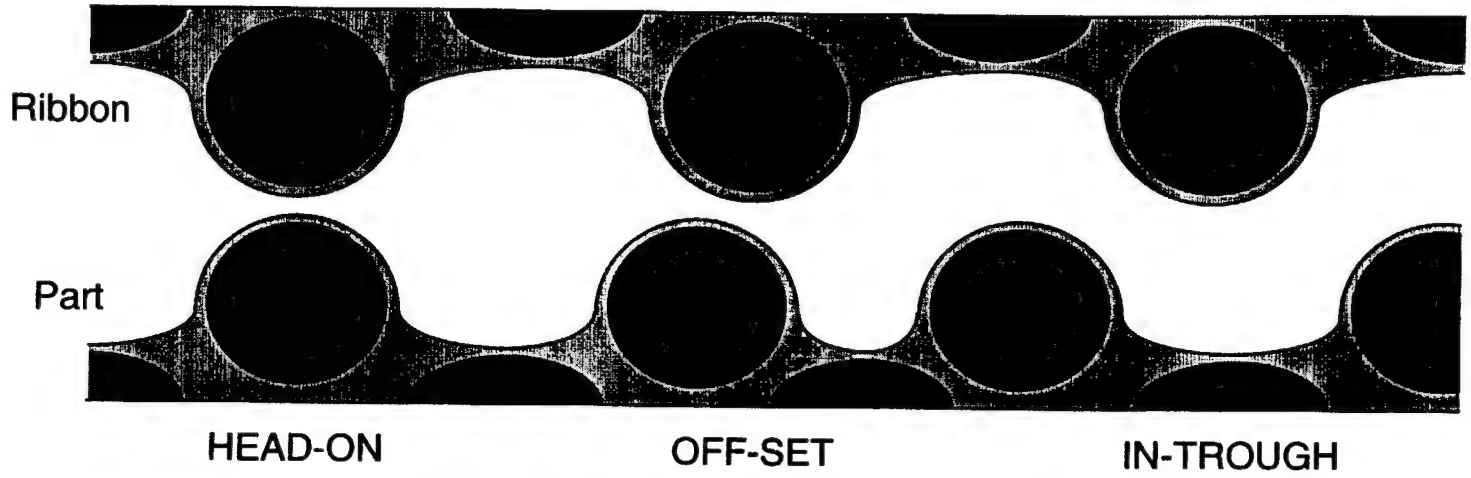

IN-LINE FIBER PLACEMENT ALIGNMENT

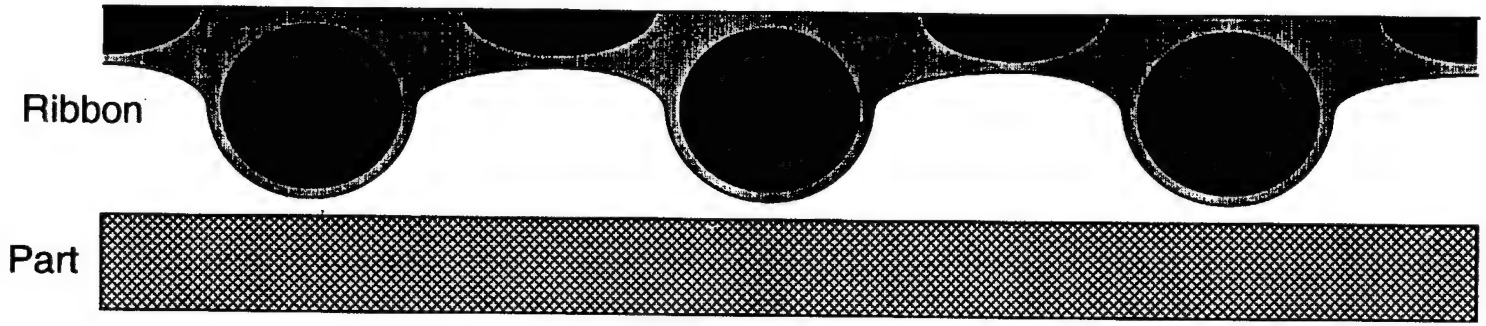

OFF-LINE FIBER PLACEMENT

INTIMATE CONTACT RIBBON SURFACE ROUGHNESS MODELS

Figure 6

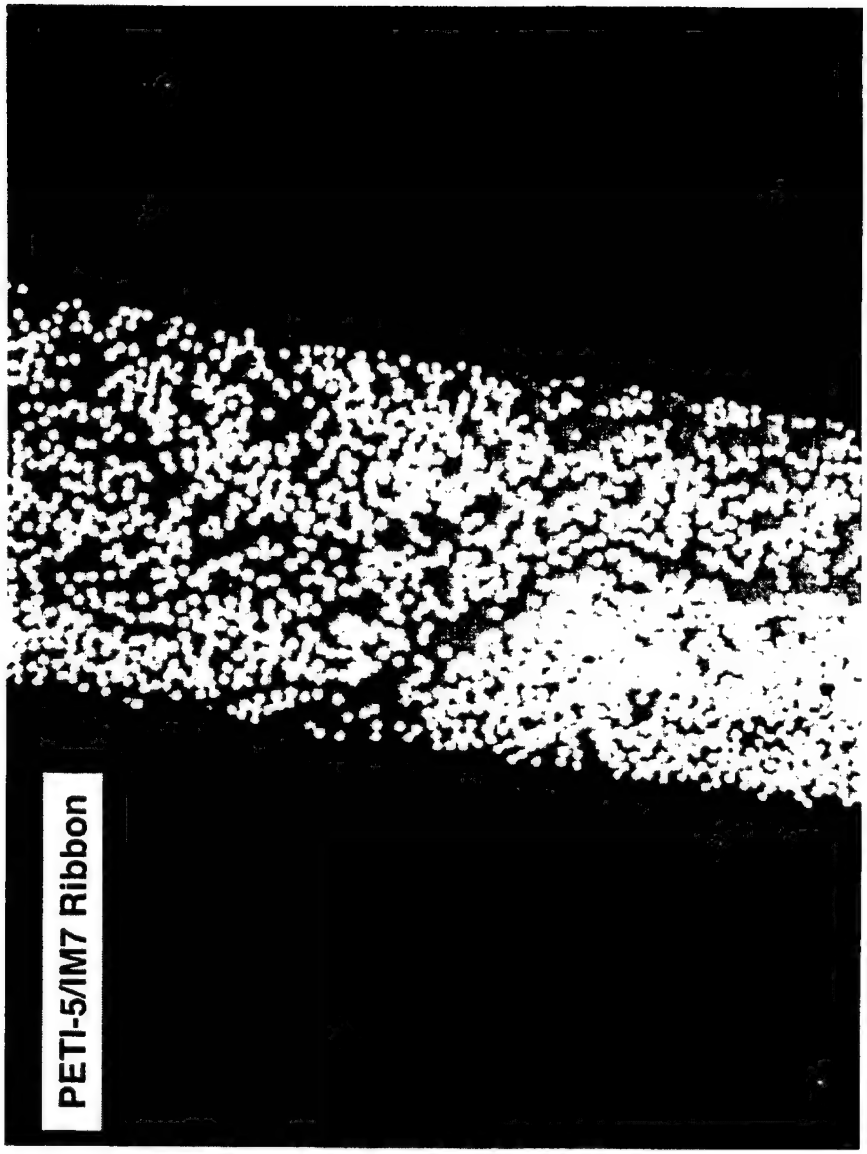

Figure 7

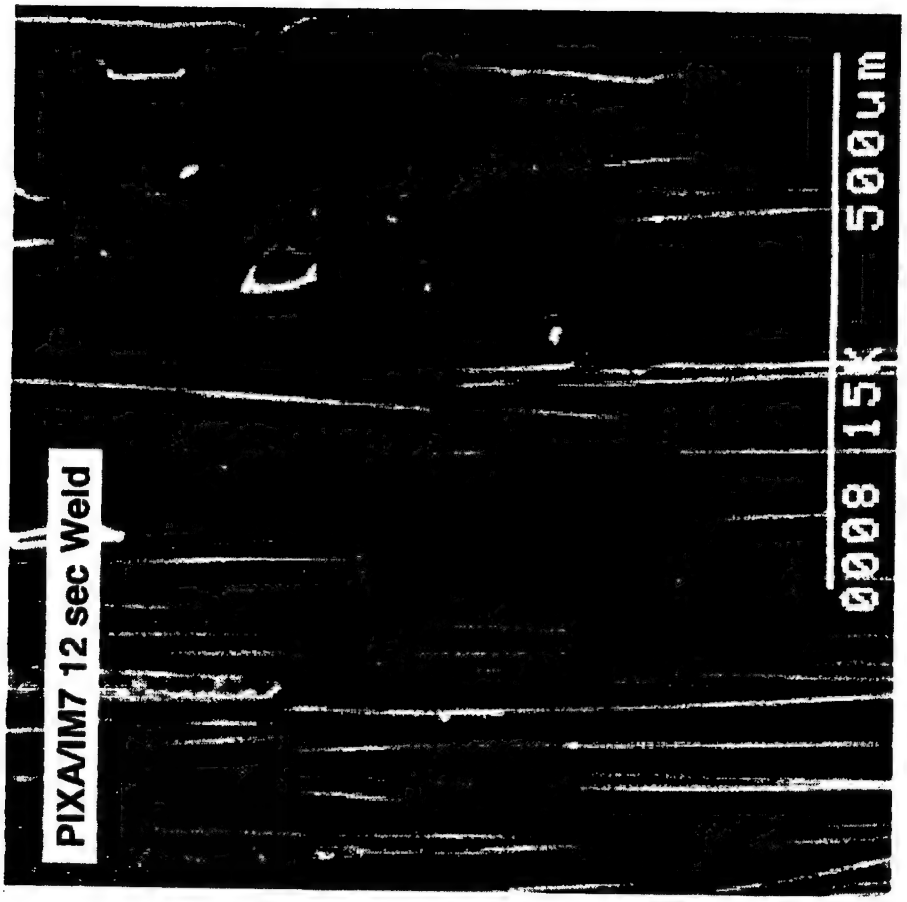

Figure 8

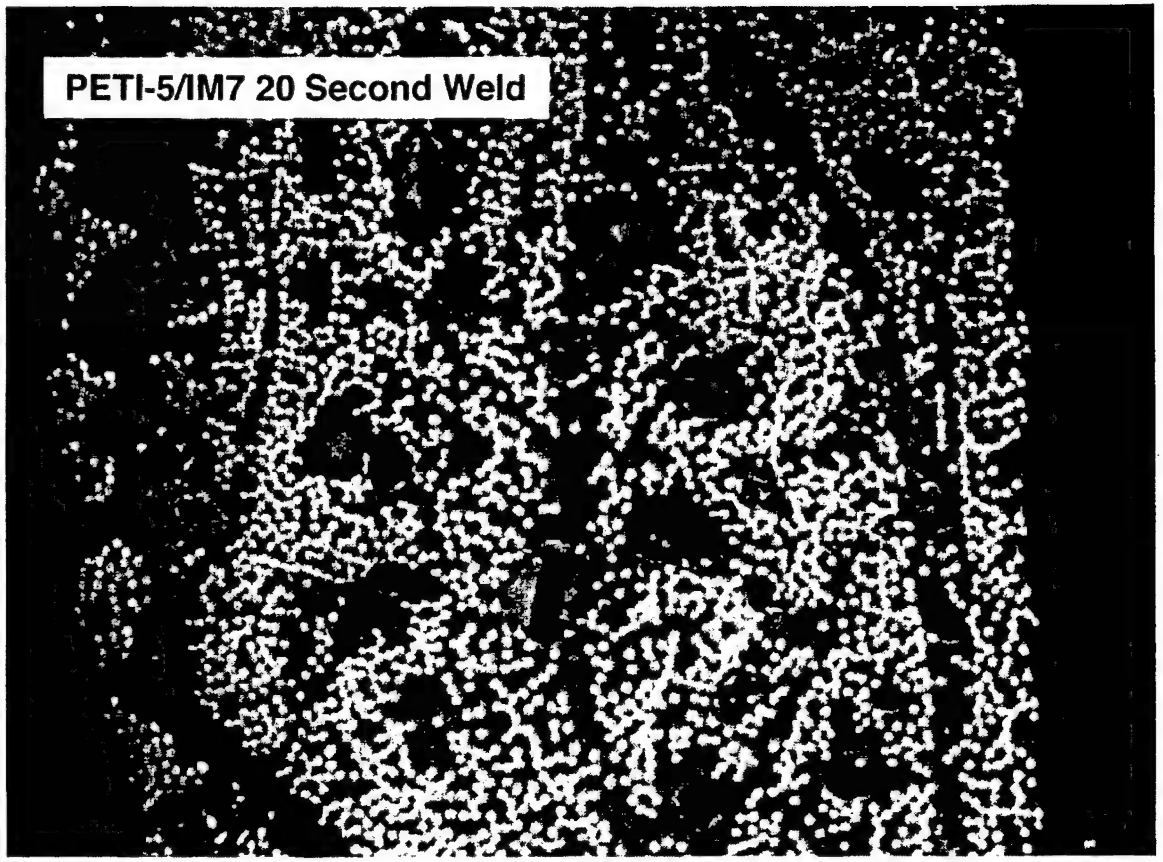

Figure 9

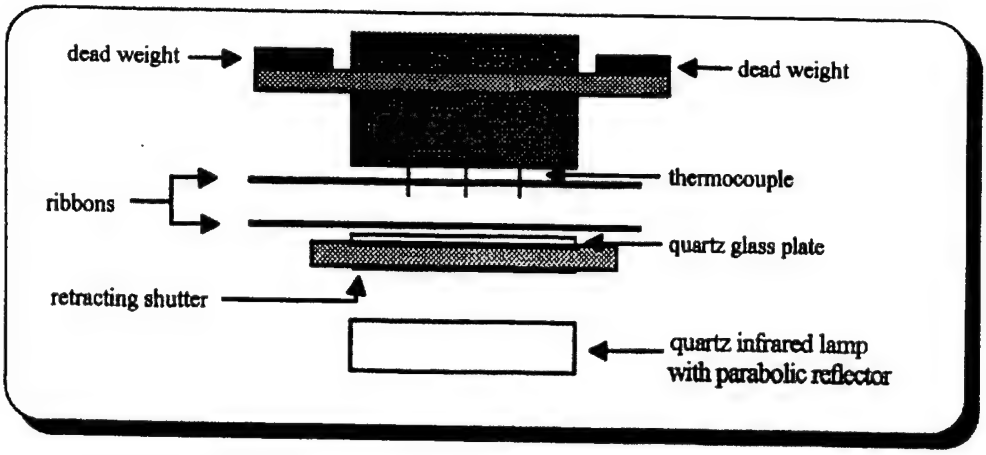
dead weight
dead weight
thermocouple
ribbons
quartz glass plate
retracting shutter
quartz infrared lamp
with parabolic reflector

Fig. 10

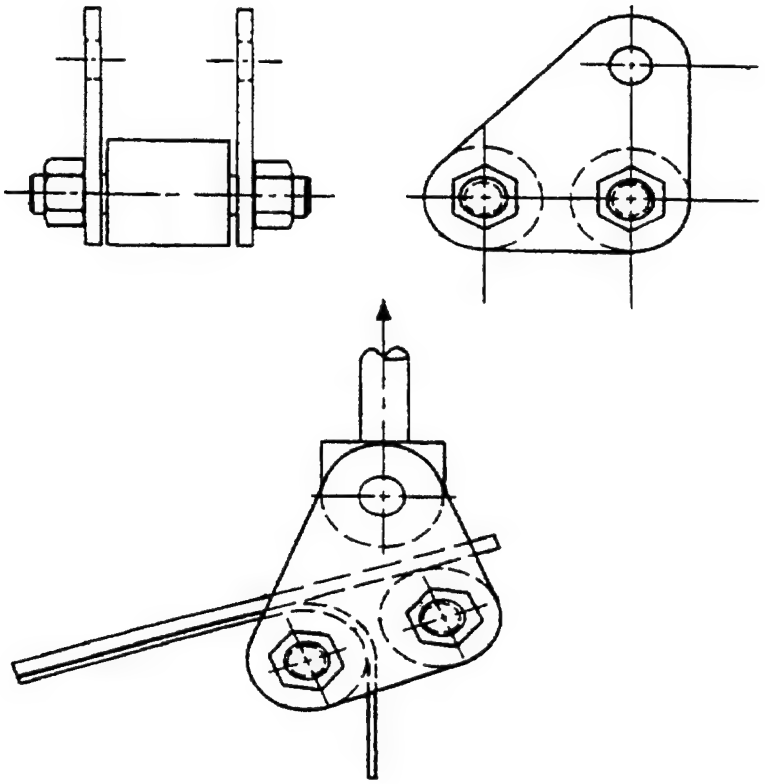

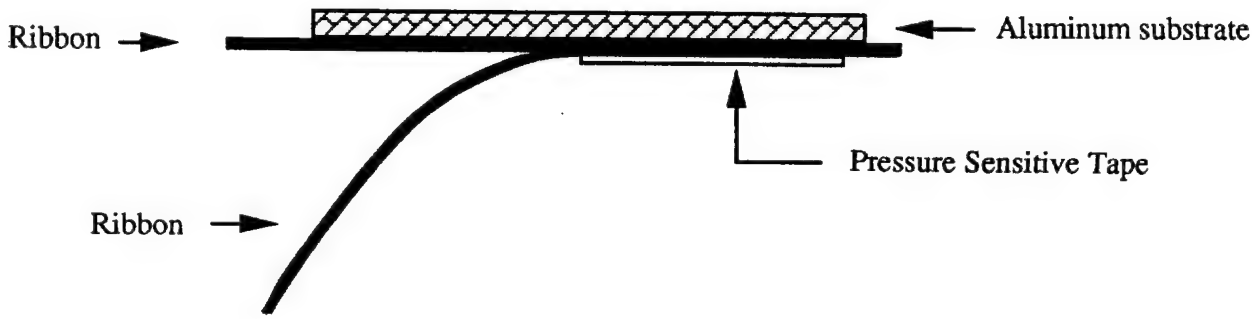
Ribbon
Aluminum substrate
Pressure Sensitive Tape
Ribbon

Fig. 11

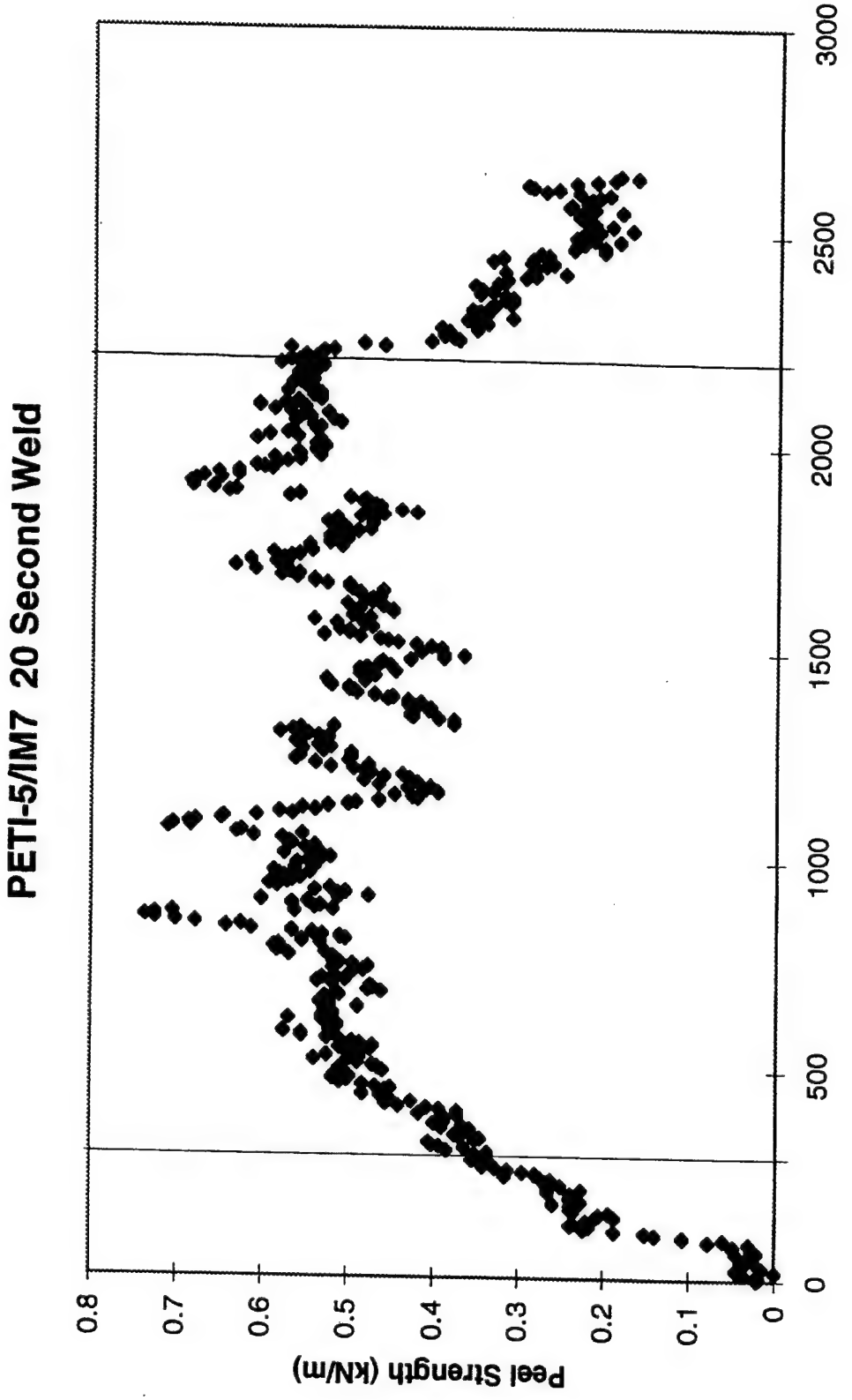
PETI-5/IM7 20 Second Weld
Peel Strength (kN/m)
0.8
0.7
0.6
0.5
0.4
0.3
0.2
0.1
0
0
500
1000
1500
2000
2500
3000

Fig. 12

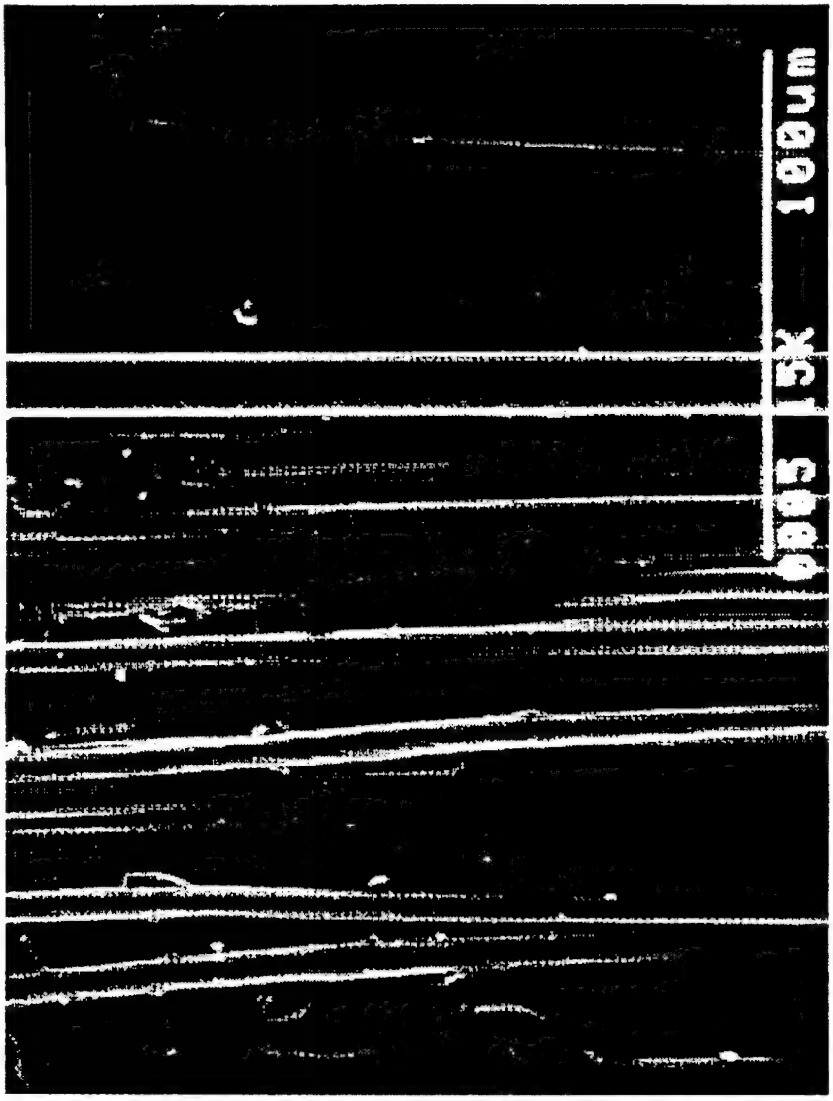

Fig. 13

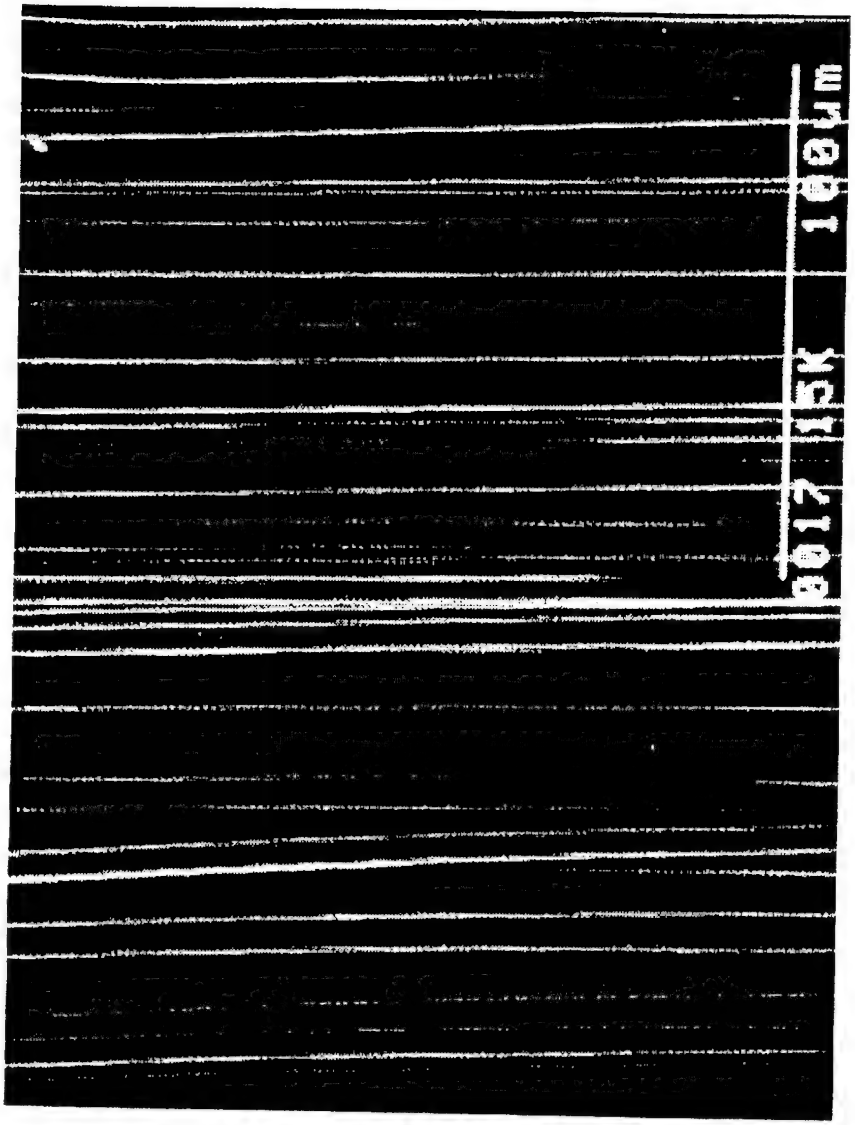

Fig. 14

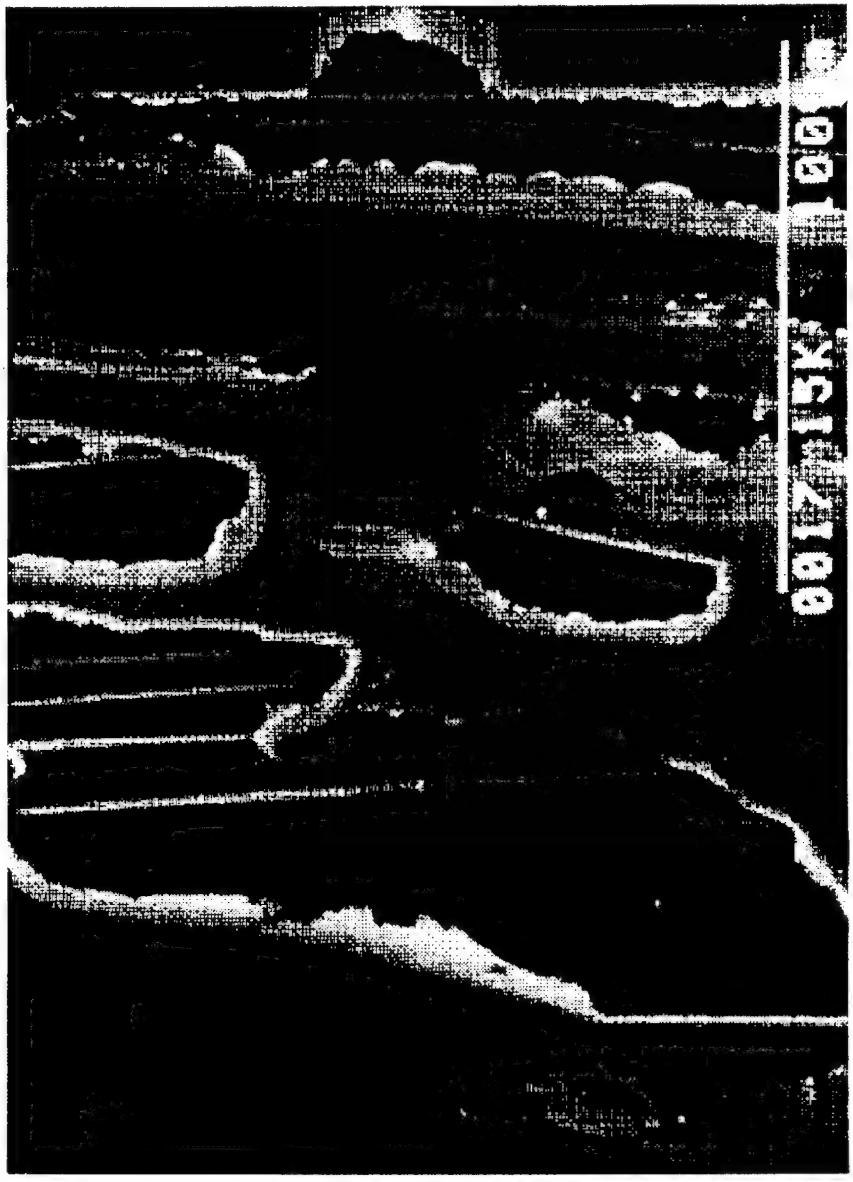

Fig. 15

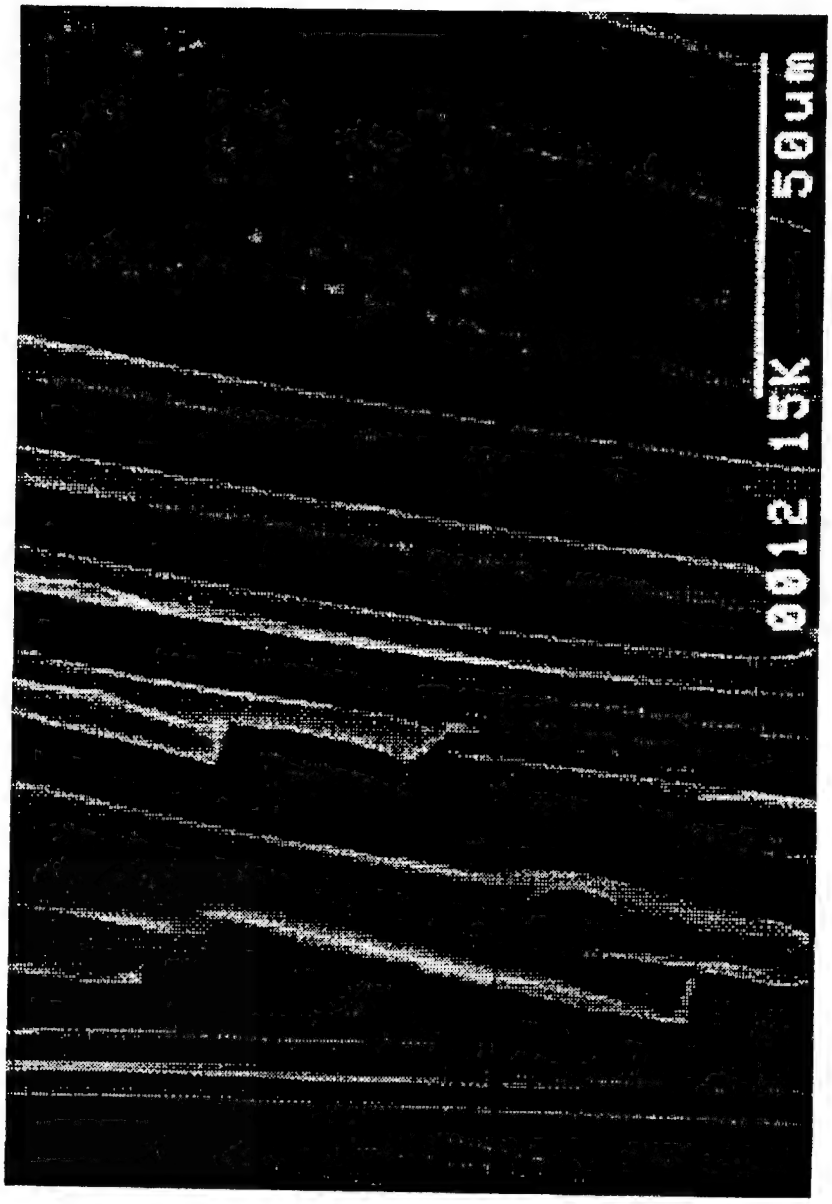

Fig. 16

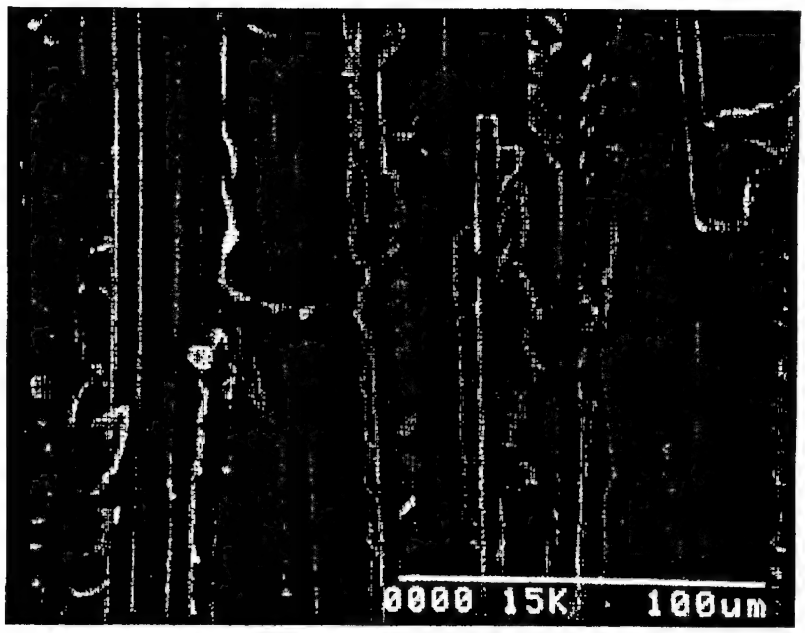

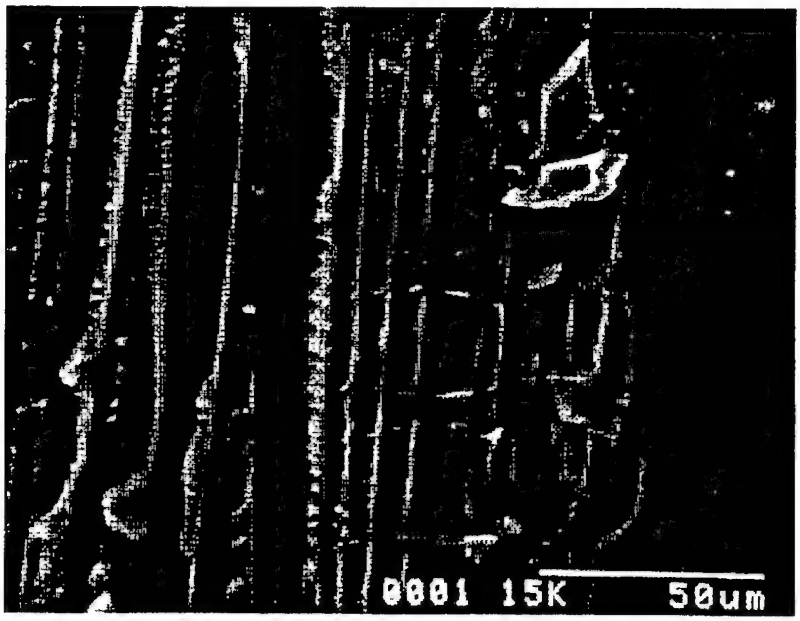

Fig. 17

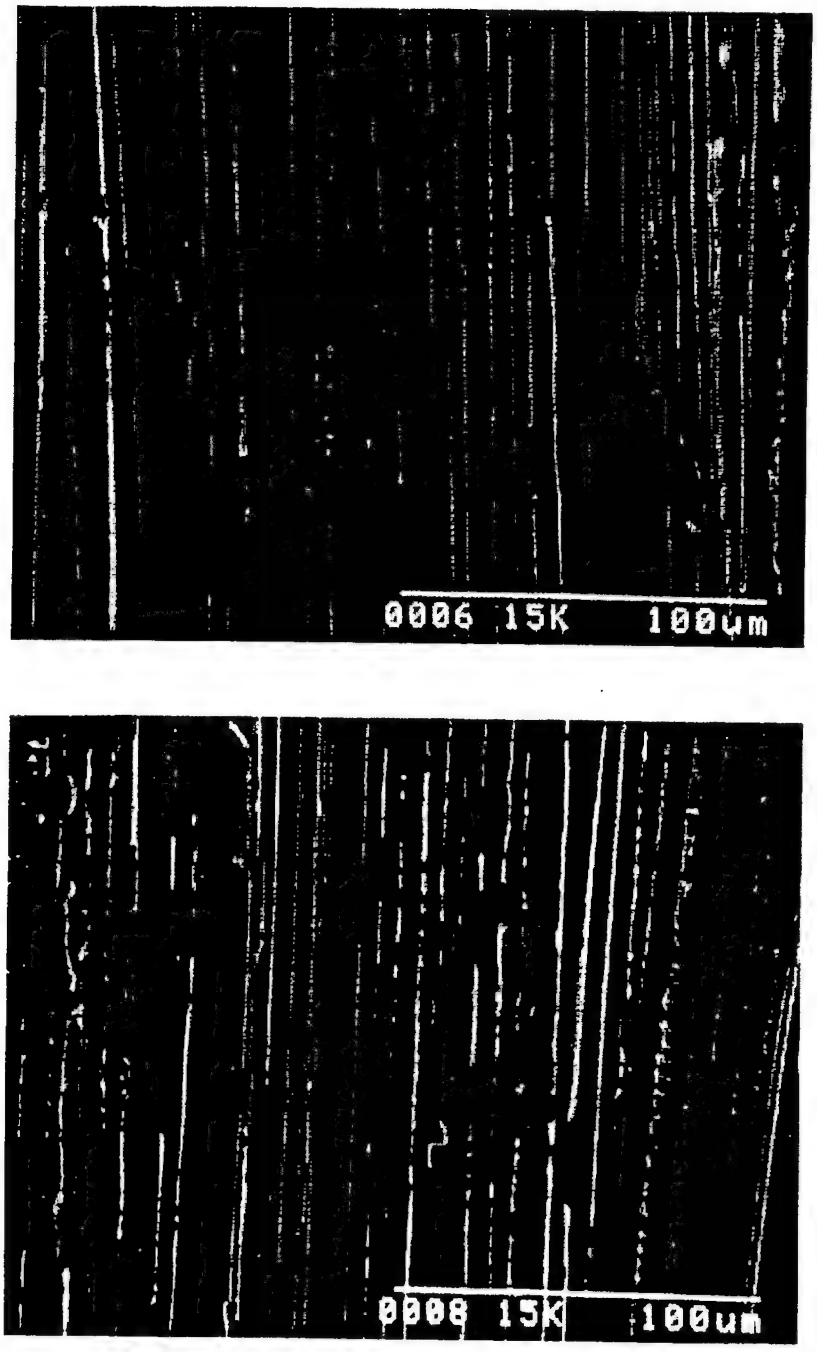

Fig. 18

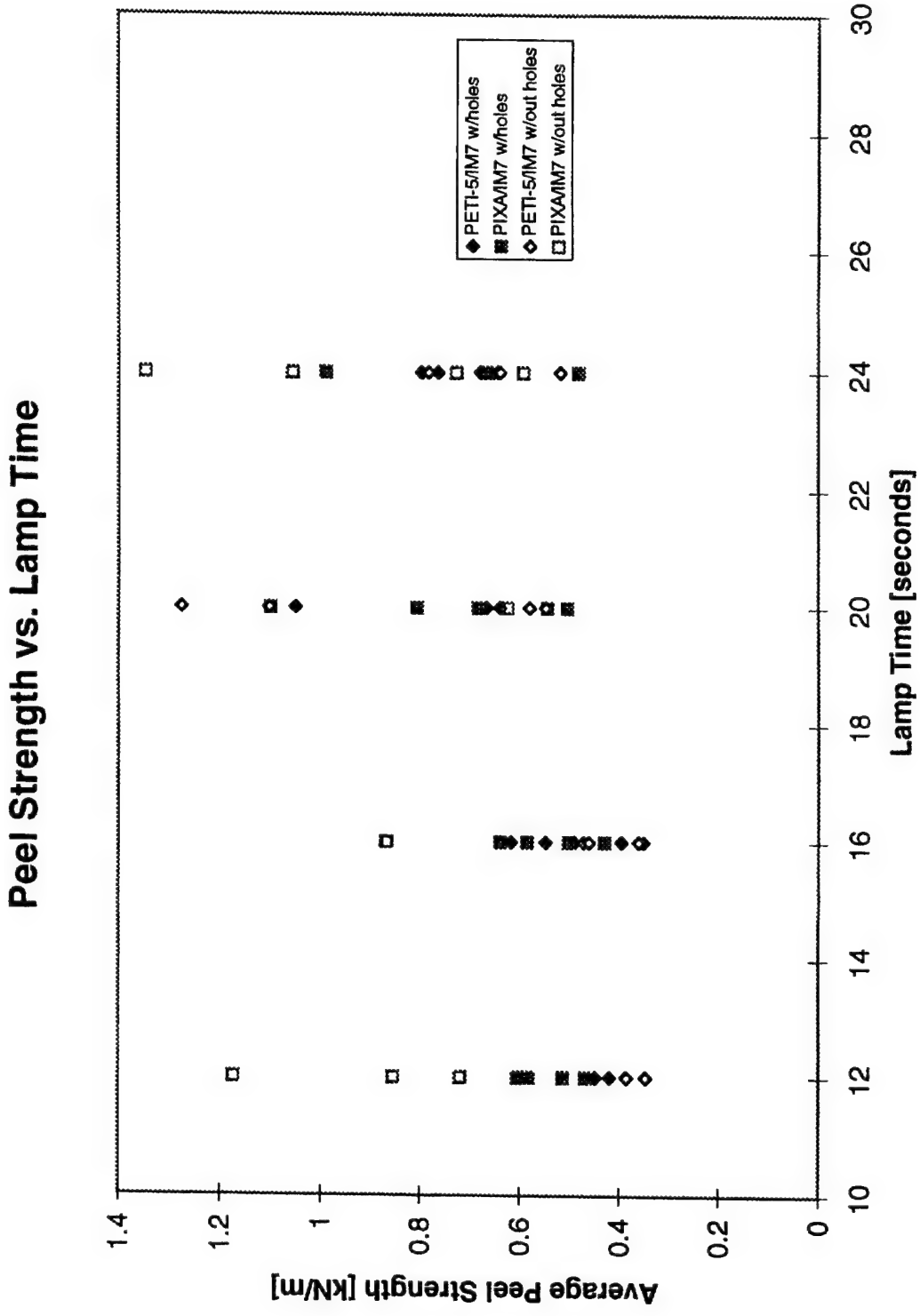
Peel Strength vs. Lamp Time
Average Peel Strength [kN/m]
Lamp Time [seconds]
PETI-5/IM7 w/holes
PIXA/IM7 w/holes
PETI-5/IM7 w/out holes
PIXA/IM7 w/out holes
0
0.2
0.4
0.6
0.8
1
1.2
1.4
10
12
14
16
18
20
22
24
26
28
30

Fig. 19

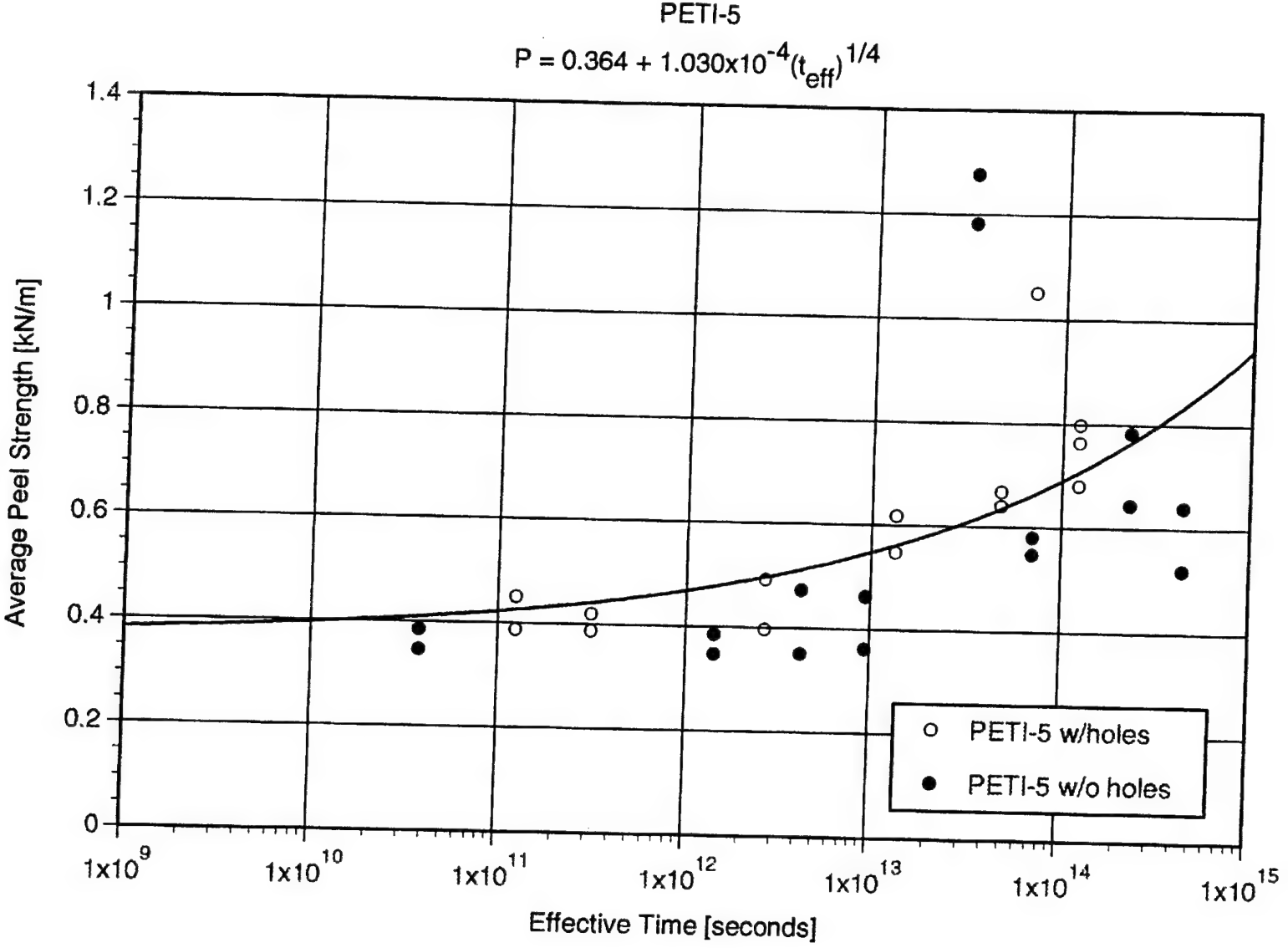
PETI-5
P = 0.364 + 1.030x10^-4(t_eff)^1/4
Average Peel Strength [kN/m]
1.4
1.2
1
0.8
0.6
0.4
0.2
0
1x10^9
1x10^10
1x10^11
1x10^12
1x10^13
1x10^14
1x10^15
Effective Time [seconds]
PETI-5 w/holes
PETI-5 w/o holes

Fig. 20

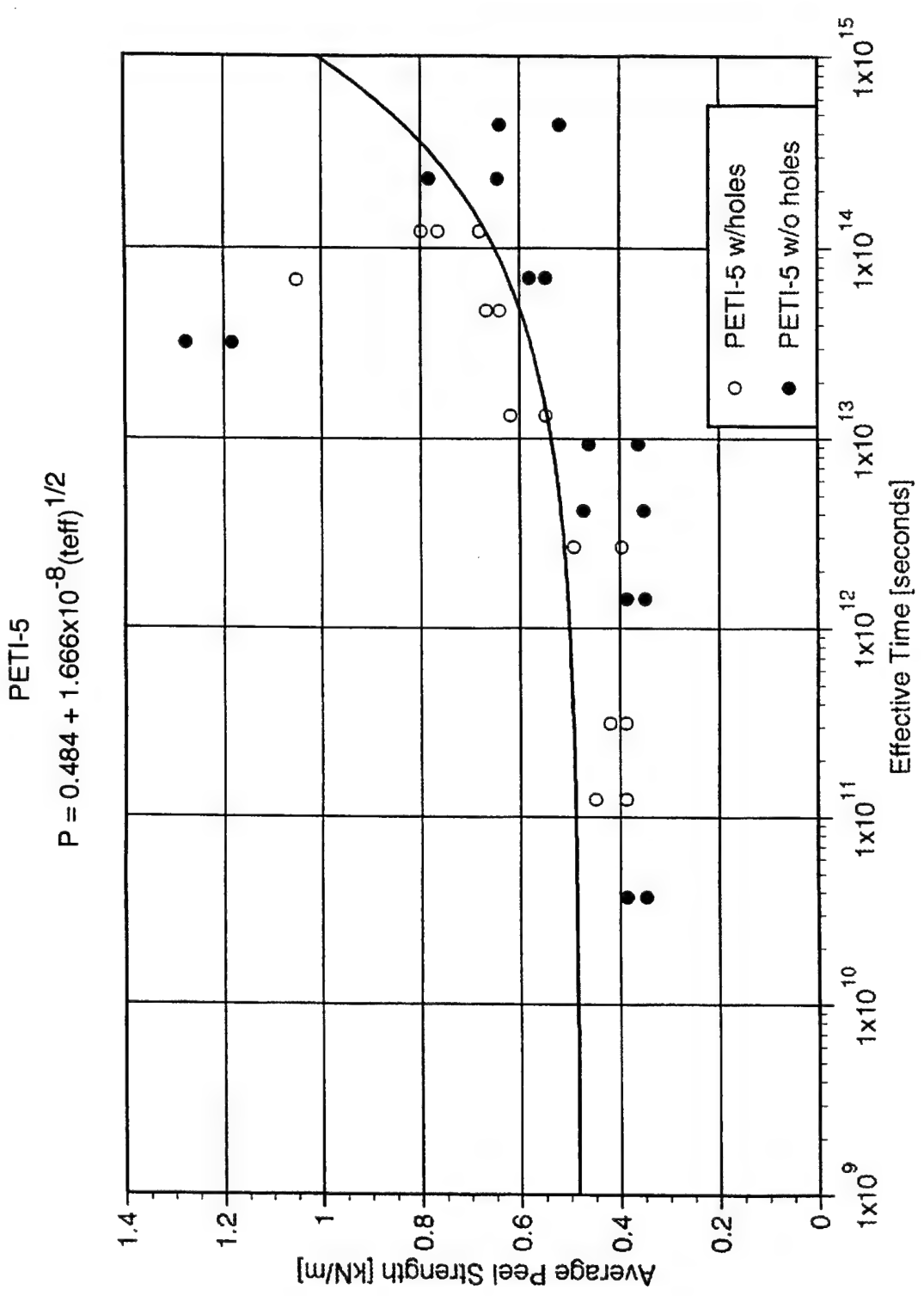
PETI-5
P = 0.484 + 1.666x10^-8(teff)^1/2
Average Peel Strength [kN/m]
Effective Time [seconds]
PETI-5 w/holes
PETI-5 w/o holes
0
0.2
0.4
0.6
0.8
1
1.2
1.4
1x10^9
1x10^10
1x10^11
1x10^12
1x10^13
1x10^14
1x10^15

Fig. 21

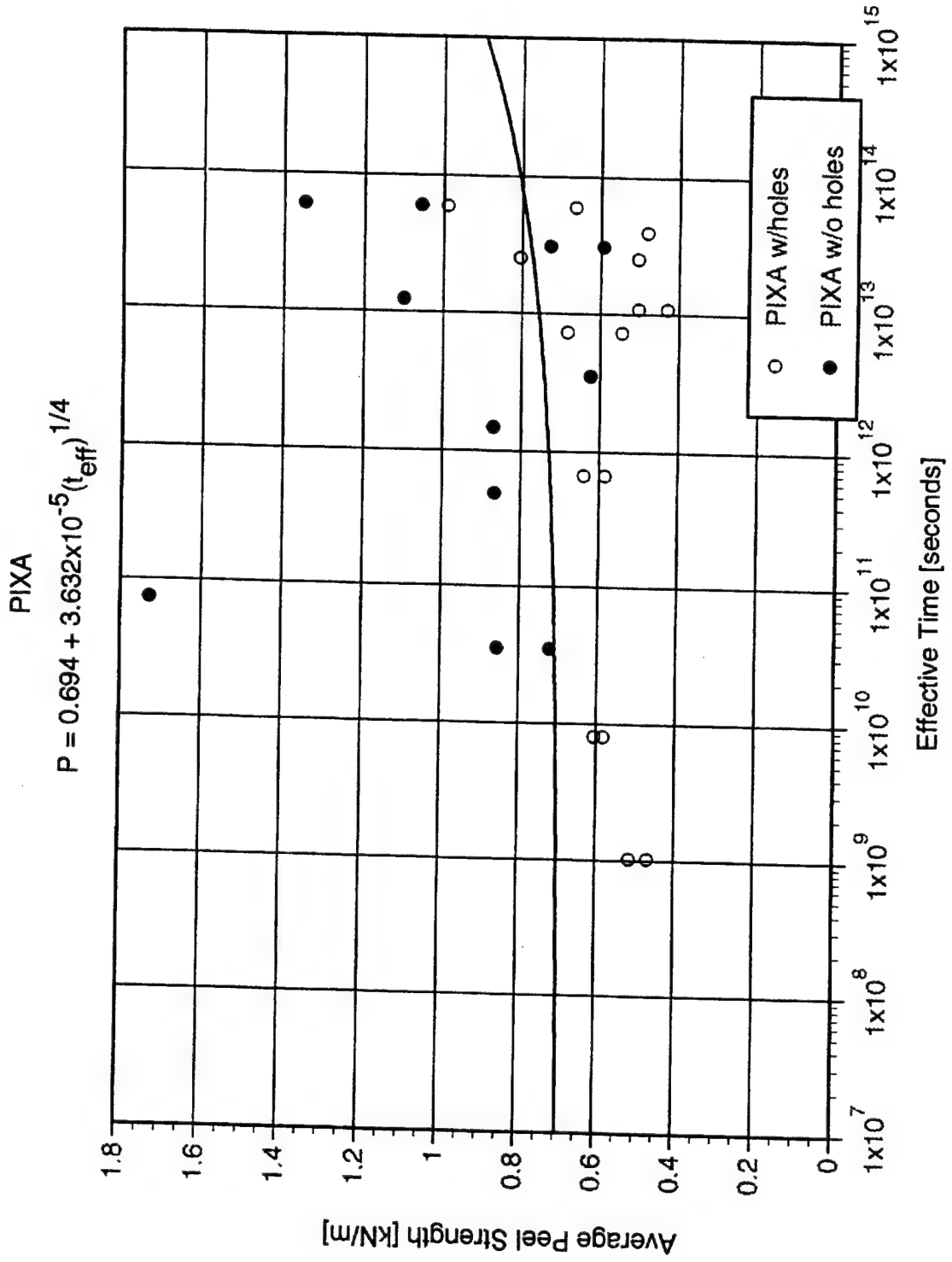
PIXA
P = 0.694 + 3.632x10^-5(t_eff)^1/4
Average Peel Strength [kN/m]
Effective Time [seconds]
PIXA w/holes
PIXA w/o holes
0
0.2
0.4
0.6
0.8
1
1.2
1.4
1.6
1.8
1x10^7
1x10^8
1x10^9
1x10^10
1x10^11
1x10^12
1x10^13
1x10^14
1x10^15

Fig. 22

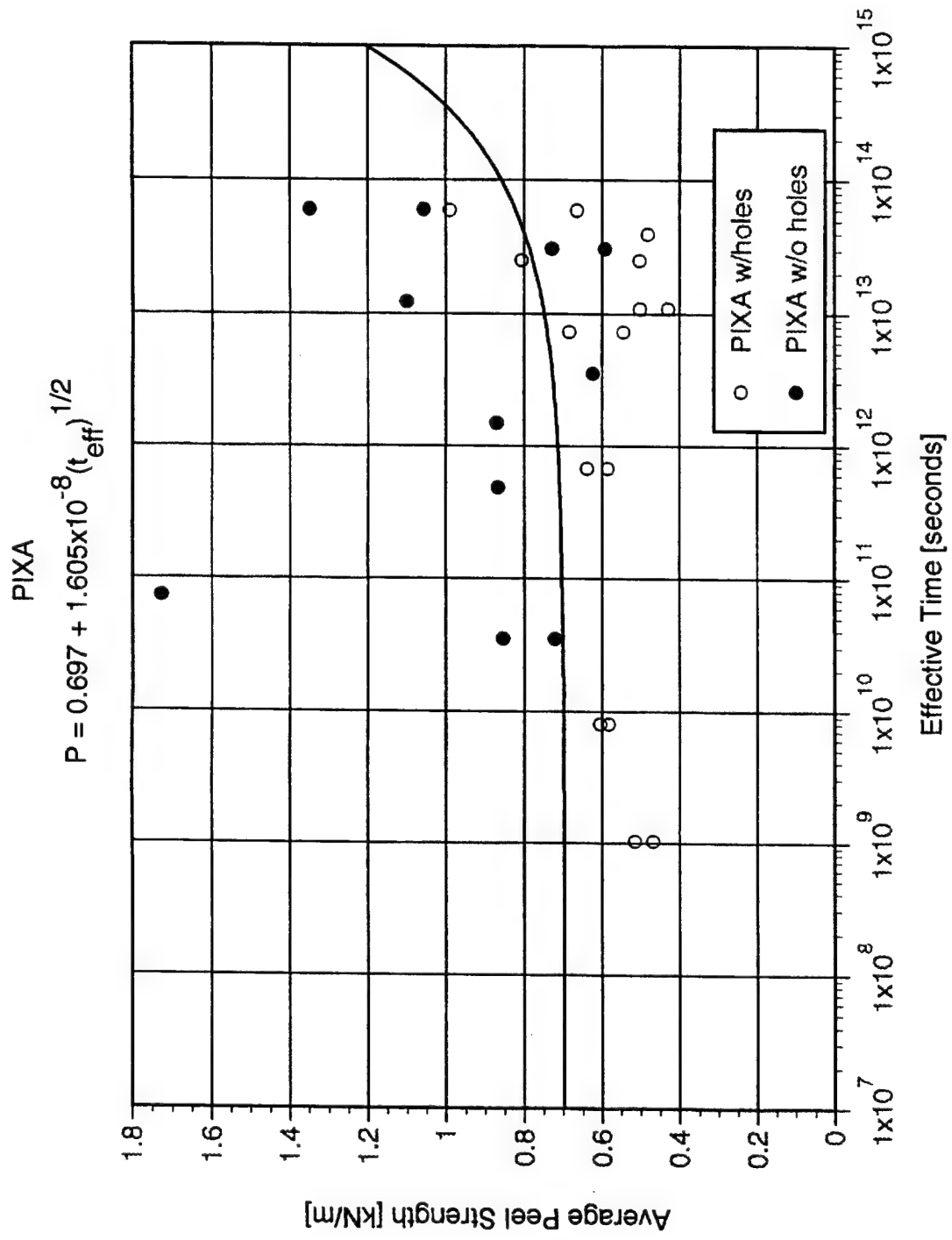
PIXA
P = 0.697 + 1.605x10^-8(t_eff)^1/2
Average Peel Strength [kN/m]
Effective Time [seconds]
PIXA w/holes
PIXA w/o holes
0
0.2
0.4
0.6
0.8
1
1.2
1.4
1.6
1.8
1x10^7
1x10^8
1x10^9
1x10^10
1x10^11
1x10^12
1x10^13
1x10^14
1x10^15

Fig. 23

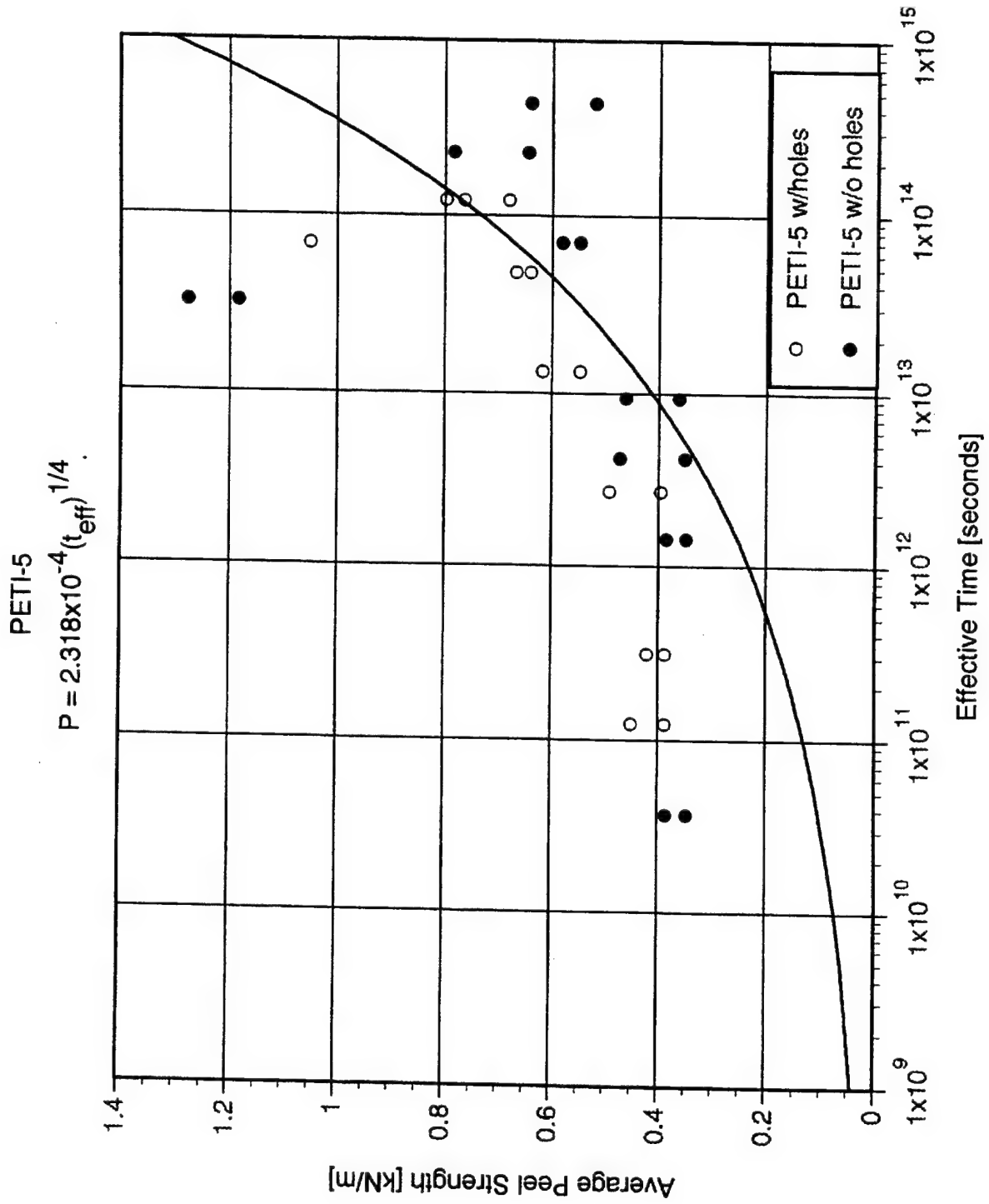
PETI-5
P = 2.318x10^-4(t_eff)^1/4
Average Peel Strength [kN/m]
Effective Time [seconds]
PETI-5 w/holes
PETI-5 w/o holes
0
0.2
0.4
0.6
0.8
1
1.2
1.4
1x10^9
1x10^10
1x10^11
1x10^12
1x10^13
1x10^14
1x10^15

Fig. 24

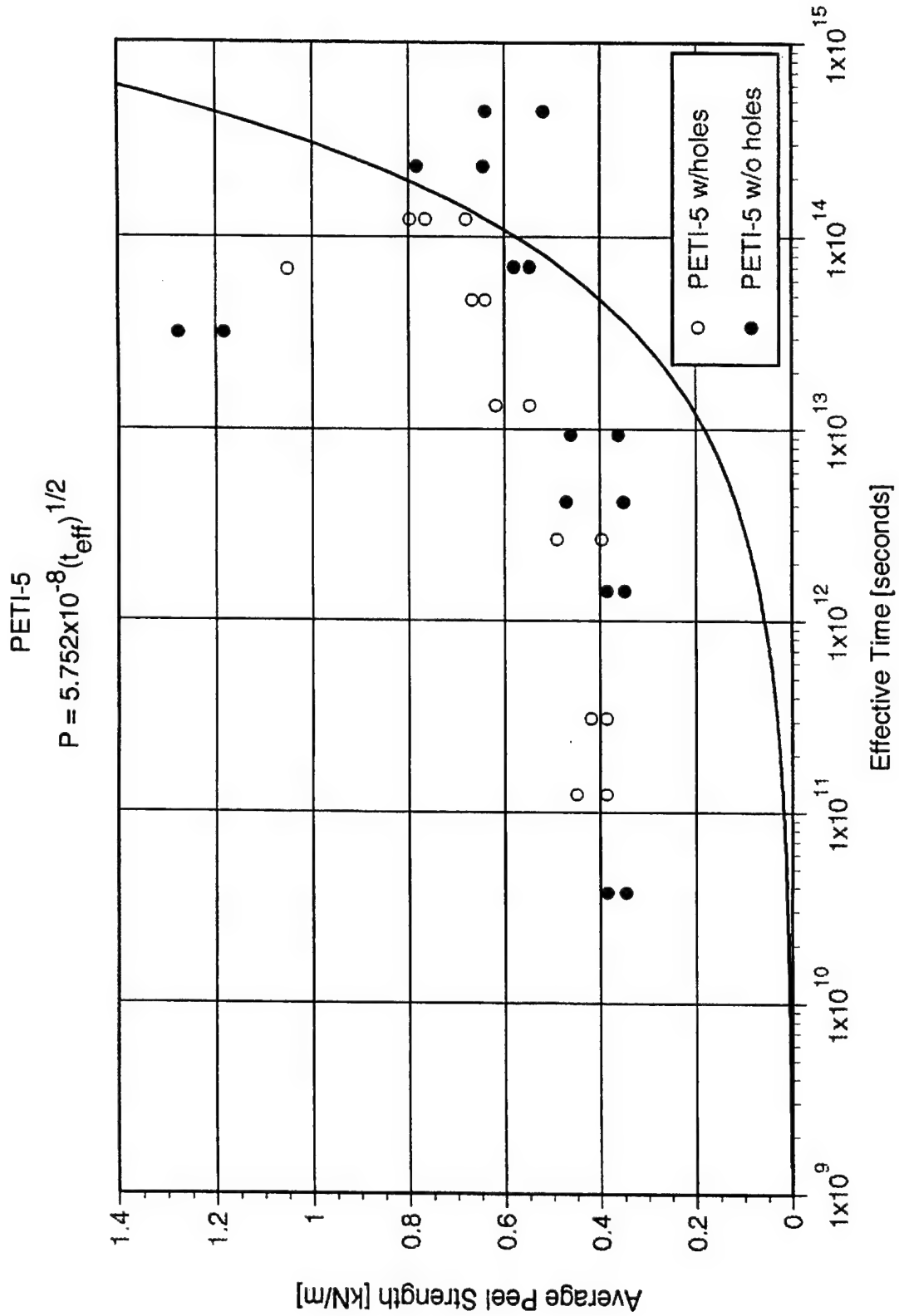
PETI-5
P = 5.752x10^-8(t_eff)^1/2
Average Peel Strength [kN/m]
Effective Time [seconds]
PETI-5 w/holes
PETI-5 w/o holes
0
0.2
0.4
0.6
0.8
1
1.2
1.4
1x10^9
1x10^10
1x10^11
1x10^12
1x10^13
1x10^14
1x10^15

Fig. 25

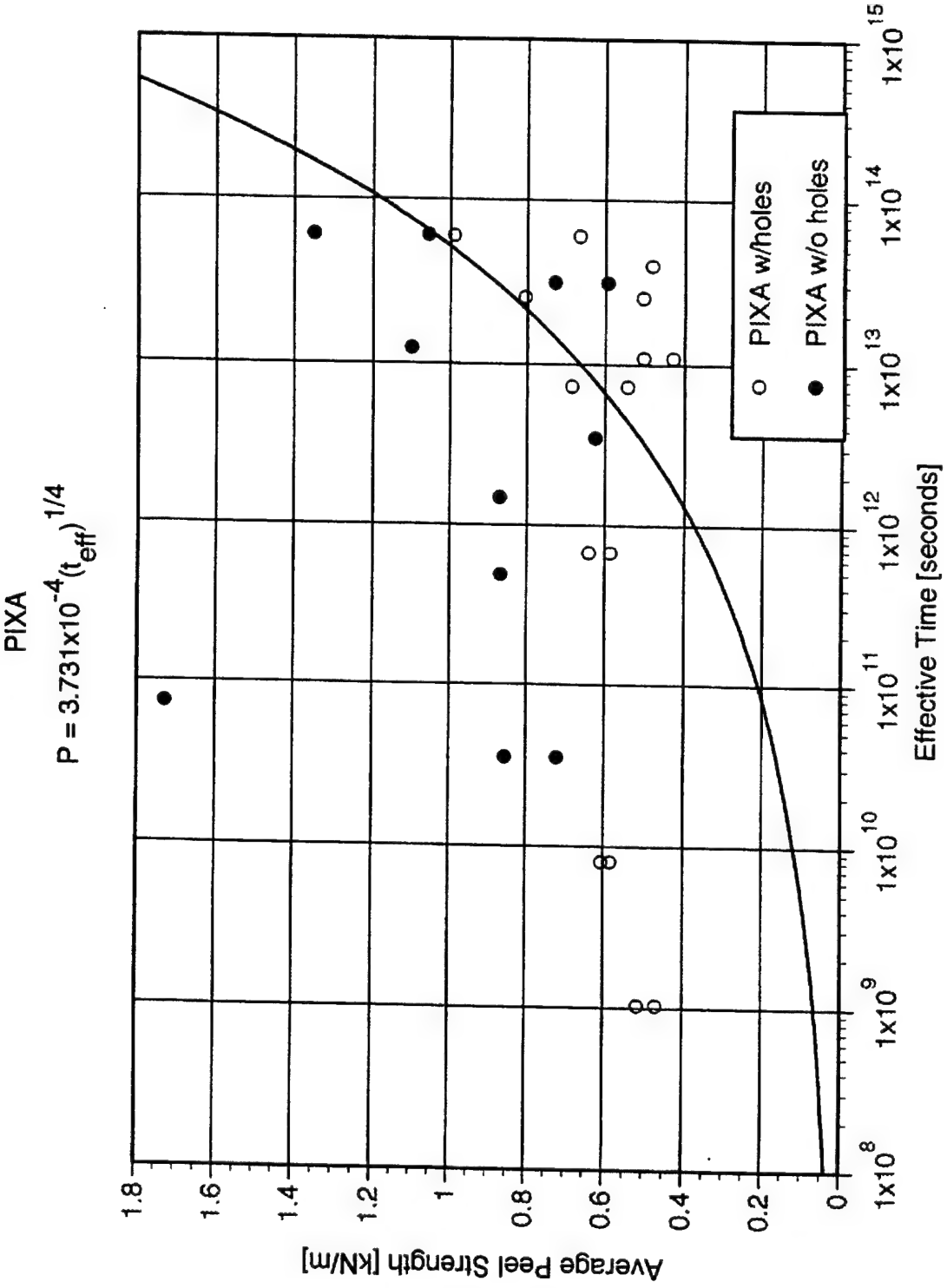
PIXA
P = 3.731x10^-4(t_eff)^1/4
Average Peel Strength [kN/m]
Effective Time [seconds]
PIXA w/holes
PIXA w/o holes
0
0.2
0.4
0.6
0.8
1
1.2
1.4
1.6
1.8
1x10^8
1x10^9
1x10^10
1x10^11
1x10^12
1x10^13
1x10^14
1x10^15

Fig. 26

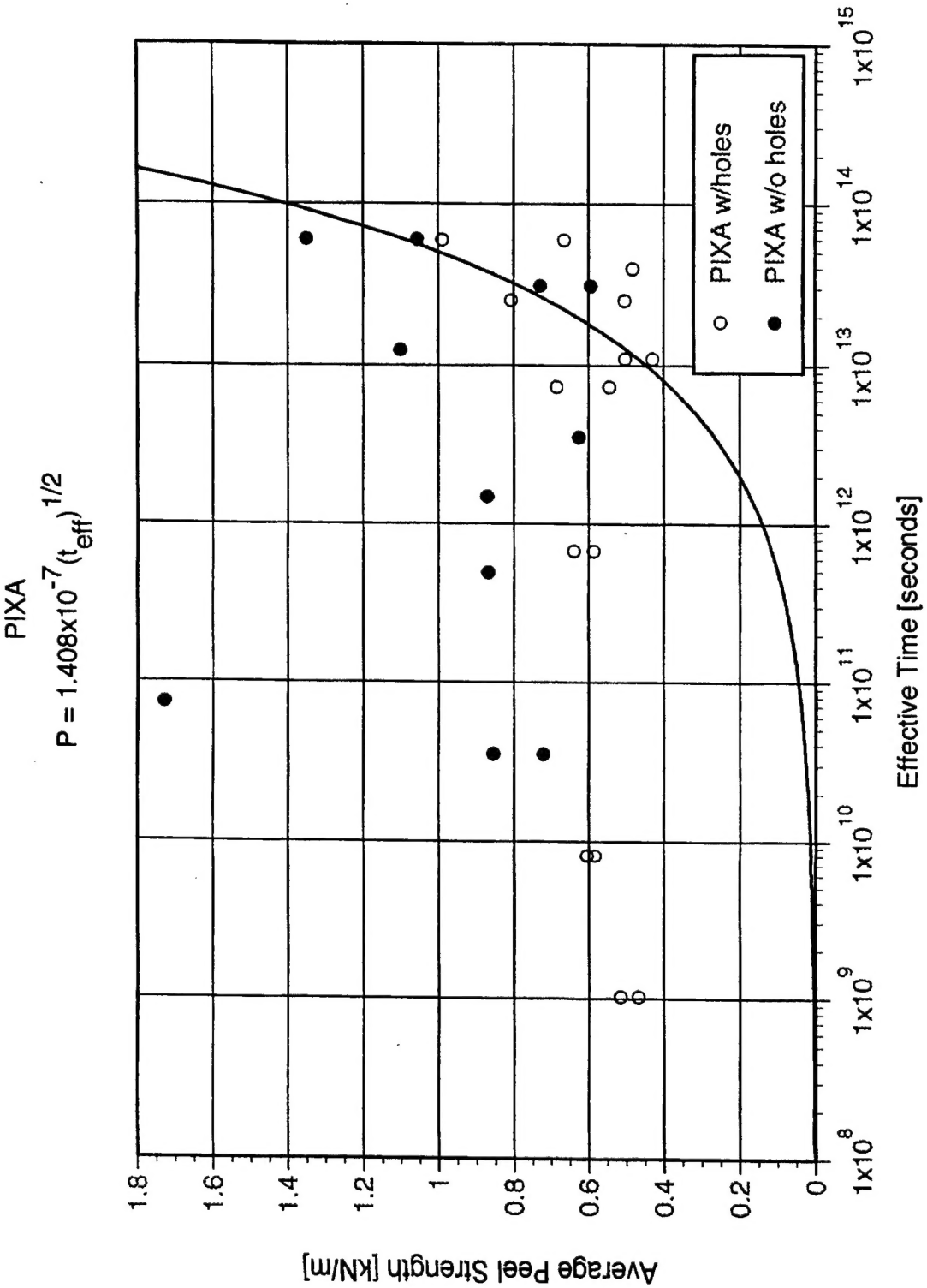
PIXA
$P = 1.408x10^{-7}(t_{eff})^{1/2}$
Average Peel Strength [kN/m]
Effective Time [seconds]
PIXA w/holes
PIXA w/o holes
0
0.2
0.4
0.6
0.8
1
1.2
1.4
1.6
1.8
$1x10^{8}$
$1x10^{9}$
$1x10^{10}$
$1x10^{11}$
$1x10^{12}$
$1x10^{13}$
$1x10^{14}$
$1x10^{15}$

Fig. 27

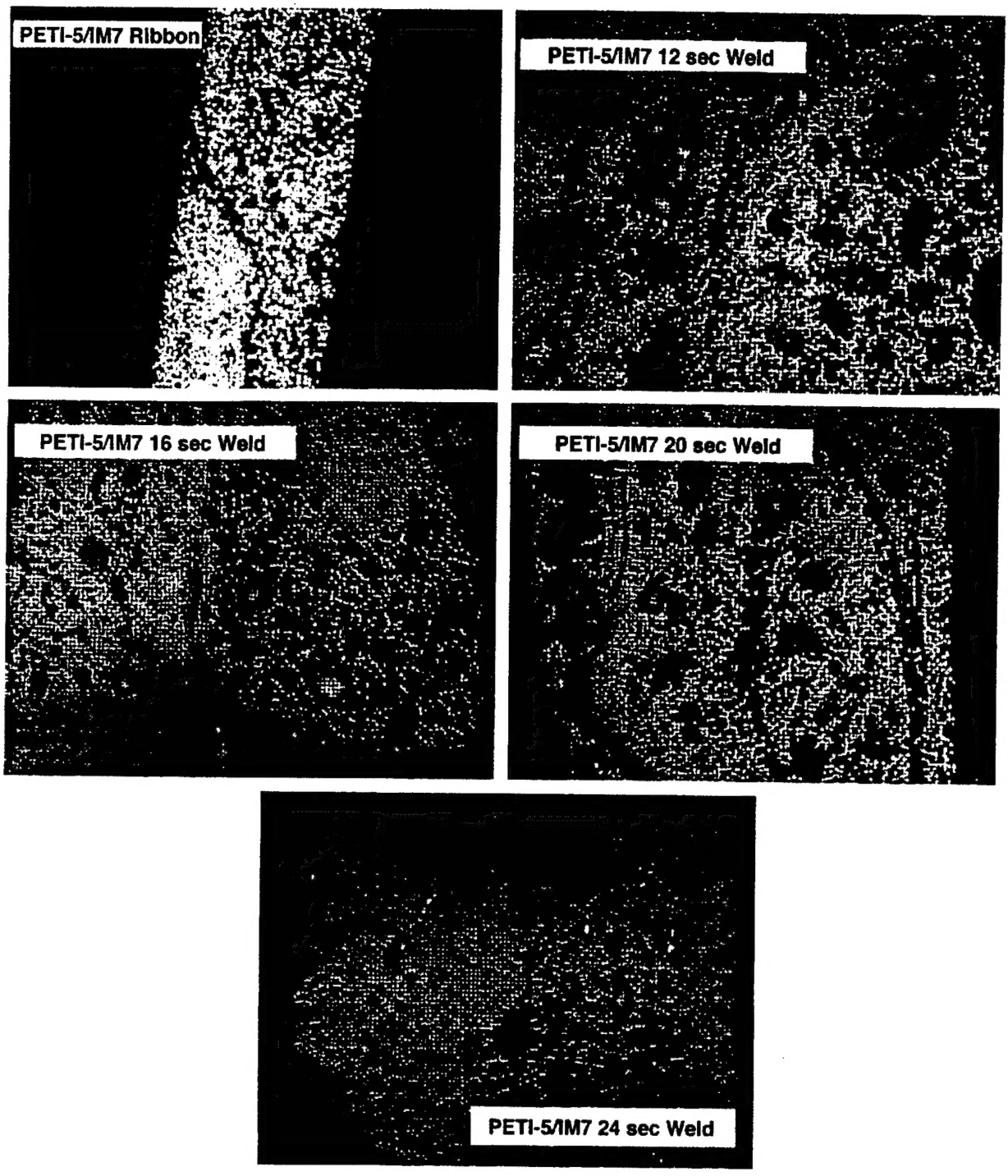
PETI-5/IM7 Ribbon
PETI-5/IM7 12 sec Weld
PETI-5/IM7 16 sec Weld
PETI-5/IM7 20 sec Weld
PETI-5/IM7 24 sec Weld

Fig. 28

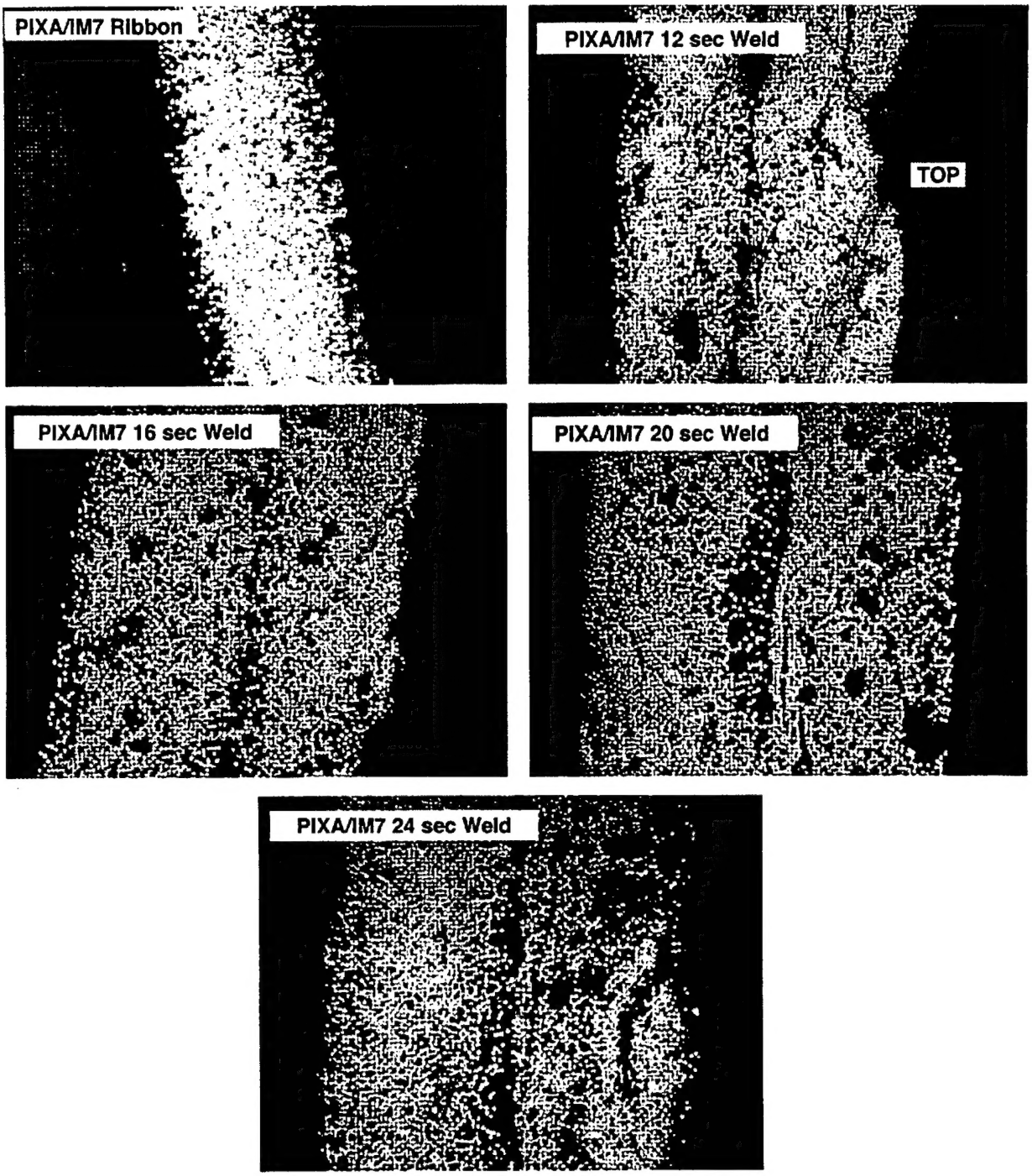
PIXA/IM7 Ribbon
PIXA/IM7 12 sec Weld
TOP
PIXA/IM7 16 sec Weld
PIXA/IM7 20 sec Weld
PIXA/IM7 24 sec Weld

Fig. 29

REPORT DOCUMENTATION PAGE

Form Approved
OMB No. 0704-0188

1. AGENCY USE ONLY *(Leave blank)*	2. REPORT DATE	3. REPORT TYPE AND DATES COVERED
	January 1996	Technical Memorandum

4. TITLE AND SUBTITLE
Thermoplastic Ribbon-Ply Bonding Model

5. FUNDING NUMBERS
505-63-50-01

6. AUTHOR(S)
Jeffrey A. Hinkley
Joseph M. Marchello
Bernadette C. Messier

7. PERFORMING ORGANIZATION NAME(S) AND ADDRESS(ES)
NASA Langley Research Center
Hampton, VA 23681-0001

8. PERFORMING ORGANIZATION REPORT NUMBER

9. SPONSORING / MONITORING AGENCY NAME(S) AND ADDRESS(ES)
National Aeronautics and Space Administration
Washington, DC 20546-0001

10. SPONSORING / MONITORING AGENCY REPORT NUMBER
NASA TM-110203

11. SUPPLEMENTARY NOTES
Hinkley: Langley Research Center, Hampton, VA
Marchello and Messier: Old Dominion University, Norfolk, VA

12a. DISTRIBUTION / AVAILABILITY STATEMENT
Unclassified - Unlimited
Subject Category - 27

12b. DISTRIBUTION CODE

13. ABSTRACT ***(Maximum 200 words)***

The aim of the present work was to identify key variables in rapid weldbonding of thermoplastic tow (ribbon) and their relationship to matrix polymer properties and to ribbon microstructure. Theoretical models for viscosity, establishment of ply-ply contact, instantaneous (Velcro) bonding, molecular interdiffusion (healing), void growth suppression, and gap filling were reviewed and synthesized.

Consideration of the theoretical bonding mechanisms and length scales and of the experimental weld/peel data allow the prediction of such quantities as the time and pressure required to achieve good contact between a ribbon and a flat substrate, the time dependence of bond strength, pressures needed to prevent void growth from dissolved moisture and conditions for filling gaps and smoothing overlaps.

14. SUBJECT TERMS
Tow placement, thermoplastic, welding, and process model.

15. NUMBER OF PAGES
60

16. PRICE CODE
A04

17. SECURITY CLASSIFICATION OF REPORT	18. SECURITY CLASSIFICATION OF THIS PAGE	19. SECURITY CLASSIFICATION OF ABSTRACT	20. LIMITATION OF ABSTRACT
Unclassified	Unclassified		